Dusty Explosions from Dusty Progenitors: The Physics of SN 2008S and the 2008 NGC 300-OT

C. S. Kochanek[1,2],

ABSTRACT

SN 2008S and the 2008 NGC 300-OT were explosive transients of stars self-obscured by very dense, dusty stellar winds. An explosive transient with an un-observed shock break-out luminosity of order $10^{10}L_\odot$ is required to render the transients little obscured and visible in the optical at their peaks. Such a large break-out luminosity then implies that the progenitor stars were cool, red supergiants, most probably $\sim 9M_\odot$ extreme AGB (EAGB) stars. As the shocks generated by the explosions propagate outward through the dense wind, they produce a shock luminosity in soft X-rays that powers the long-lived luminosity of the transients. Unlike typical cases of transients exploding into a surrounding circumstellar medium, the progenitor winds in these systems are optically thick to soft X-rays, easily absorb radio emission and rapidly reform dust destroyed by the peak luminosity of the transients. As a result, X-rays are absorbed by the gas and the energy is ultimately radiated by the reformed dust. Three years post-peak, both systems are still significantly more luminous than their progenitor stars, but they are again fully shrouded by the re-formed dust and only visible in the mid-IR. The high luminosity and heavy obscuration may make it difficult to determine the survival of the progenitor stars for ~ 10 years. However, our model indicates that SN 2008S, but not the NGC 300-OT, should now be a detectable X-ray source. SN 2008S has a higher estimated shock velocity and a lower density wind, so the X-rays begin to escape at a much earlier phase.

Subject headings: stars: evolution – supergiants – supernovae:general

1. Introduction

SN 2008S (Arbour & Boles 2008) and the 2008 NGC 300-OT ("optical transient", Monard 2008) were initially classified as unremarkable Type IIn transients that were likely massive star eruptions rather than true supernovae (Steele et al. 2008, Bond et al. 2008). However, searches for optical progenitors proved fruitless (Prieto et al. 2008b, Berger & Soderberg 2008), which was peculiar because the transients were little obscured and a massive star should have been easily visible. It became clear that they represented a new class of massive star transients when Prieto (2008a) and Prieto et al. (2008b) identified the progenitors in archival Spitzer data as completely obscured stars with luminosities of order $60000L_\odot$ and apparent photospheric temperatures of order 400 K. In mid-IR color-magnitude diagrams, the stars lie at the

[1]Department of Astronomy, The Ohio State University, 140 West 18th Avenue, Columbus OH 43210

[2]Center for Cosmology and AstroParticle Physics, The Ohio State University, 191 W. Woodruff Avenue, Columbus OH 43210

extreme limit of the asymptotic branch (AGB) and they are extremely rare, with only 1–10 similar stars per galaxy (Thompson et al. 2009, Khan et al. 2010). Thompson et al. (2009) suggested that the M85-OT-2006, SN 1999bw, and SN 2002bu are also likely members of this class, and Kasliwal et al. (2011) propose PTF10FQS as a member. They are clearly not members of the "luminous red nova" population represented by V838 Mon and V4332 Sgr (Kulkarni et al. 2007). Our working hypothesis, which is by no means universally accepted, is that the progenitors are extreme AGB (EAGB) stars with masses of order $M_* \simeq 9M_\odot$ cloaked by extremely dense $\dot{M} \sim 10^{-4}M_\odot$/year winds.

While a few studies have focused on "traditional" optical examinations of these transients (Berger et al. 2009, Smith et al. 2009, Smith et al. 2010), it is impossible to understand even their energetics without the addition of near-IR and mid-IR data (Bond et al. 2009, Botticella et al. 2009, Prieto et al. 2009, Ohsawa et al. 2010, Prieto et al. 2010, Wesson et al. 2010, Hoffman et al. 2011, Prieto et al. 2011). Not only is the near/mid-IR emission significant at peak, but it increasingly dominates the emission as time passes, to the point where both transients are again invisible in the optical and near-IR but remain significantly more luminous than their progenitors in the mid-IR (Prieto et al. 2010, Hoffman et al. 2011, Prieto et al. 2011). Thus, one goal of the present effort is to provide a self-consistent model of the evolving spectral energy distributions (SED) of these transients.

Unfortunately, there are two possible masses that can be associated with evolved stars having the luminosities of the progenitors. They can be cold (3000 K) EAGB stars with $M_* \simeq 9M_\odot$ or hotter (> 7500 K) $\sim 15M_\odot$ stars, but we have no direct information on the progenitor temperatures because of the obscuration. In Thompson et al. (2009) we argued for the lower mass scale because extreme AGB stars are expected to be heavily obscured by dusty winds while the more massive stars are not (e.g. Poelarends et al. 2008). This is supported by the lack of silicate features in the SEDs (e.g. Wesson et al. 2010) or in the IRS spectrum of the NGC 300-OT (Prieto et al. 2009), since EAGB stars generally have graphitic dusts while massive stars have silicate dusts (e.g. Groenewegen et al. 2009). Umana et al. (2010), further cited by Smith et al. (2010), note the presence of PAH-related features in mid-IR spectra of a candidate Luminous Blue Variable (LBV), and thus argue that some more massive stars may also have graphitic dusts. However, Prieto et al. (2009) already noted that some massive stars have graphitic dust features, but none unite the key points about the NGC 300-OT spectrum: the absence of silicate features, the presence of graphitic features and that the wavelengths of the graphitic features are indicative of predominantly aliphatic hydrocarbons rather than PAHs, which implies formation in an environment with little UV radiation. This favors the EAGB model independent of the composition. The highest mass stars observed near the transients can be used to estimate an upper, *but not a lower*, bound on the masses of the stars, and there are stars as massive as 15-20$M_\odot$ near the NGC 300-OT (Gogarten et al. 2009) but not near SN 2008S (Prieto et al. 2011). Because this approach supplies only upper bounds, these results again favor the lower mass EAGB stars if the two transients have a common physical origin. Proponents of the higher mass progenitors (Bond et al. 2009, Smith et al. 2009, Berger et al. 2009), also favor models in which the progenitor is obscured by a shell of previously ejected material, similar to IRC+10420 (e.g. Humphreys et al. 1997), rather than a steady state wind. The lack of mid-IR variability from the progenitors (Prieto et al. 2008b, Thompson et al. 2009) largely ruled out absorption in an expanding shell since the expansion should have led to an observable drop in the dust temperature over the duration

of the archival observations of the progenitors, again favoring the dense winds observed around EAGB stars. We will find that the nature of the transient both constrains the radius of the progenitor star to be very large and requires the existence of a very dense wind, further reinforcing the EAGB hypothesis.

The nature of the transients is also debated. In Thompson et al. (2009) we outlined a broad range of possibilities including stellar eruptions, sub-luminous SN and the final phases of stripping stars to leave a massive white dwarf. Potentially the most interesting of these possibilities is an electron capture SN (ecSN), since they are predicted to be sub-luminous and associated with EAGB stars (e.g. Pumo et al. 2009). Bond et al. (2009), Berger et al. (2009) and Smith et al. (2009) firmly favor non-explosive, stellar eruptions, Botticella et al. (2009) favored the ecSN scenario and Kashi et al. (2010) suggested binary interactions. At present, the only evidence against explosive transients is the failure to detect either X-ray or radio emission (Chandra & Soderberg 2008, Botticella et al. 2009, Berger et al. 2009). The present day obscuration and luminosities mean that the simplest test of these hypothesis, the survival of the progenitor, cannot be carried out. While we will be unable to answer this question precisely, we will find the transients had to be explosive in nature.

Our goal here is to combine the available observations of the progenitors and the transients to produce a self-consistent model that addresses the puzzles about these events outlined above. We make only three hypotheses. First, the progenitors were obscured by dense dusty winds, whose properties we constrain in §2. Second, that the transient ejected a significant amount of mass at velocities characterized by the 500-1000 km/s velocities observed near the transient peak (Botticella et al. 2009, Bond et al. 2009, Smith et al. 2009 Berger et al. 2009, Smith et al. 2010). Third, that the dust destroyed by the transient subsequently reforms. Section §3 combines these elements to build quantitative models of the transient light curves in terms of the evolution of the luminosity, shock radius, characteristic dust radius, and dust optical depth. In §4 we examine the physical consequences of the model. In §4.1 we show how the destruction of dust needed to render the transients optically visible at peak requires an explosive transient from a cool, red supergiant. In §4.2 we discuss recombination, cooling and dust re-formation in the wind exterior to the expanding shock. In §4.3 we propose that the late time luminosity is powered by X-ray emission from shock heating the dense wind that is subsequently absorbed and finally escapes in the mid-IR. We also predict the X-ray emissions, finding that while neither source should have been detected in existing X-ray observations, SN 2008S should now be a detectable X-ray source while the NGC 300-OT should not. Similarly, we expect early phase radio emission to be absorbed. Finally, in §4.4 we discuss the expected evolution of the optical, near-IR and mid-IR emissions and in §4.5 the possibilities for detecting surviving progenitor stars. In §5 we summarize the results, relate them to other similar transients and discuss future tests of the hypothesis. We adopt distances of 1.88 Mpc for NGC 300 (Gieren et al. 2005) and 5.6 Mpc for SN 2008S in NGC 6946 (Sahu et al. 2006) and Galactic foreground extinctions of $E(B-V) = 0.013$ and 0.342 based on Schlegel et al. (1998).

2. The Progenitors

An EAGB star is surrounded by a radiatively accelerated wind of mass loss rate $\dot{M}$ and asymptotic velocity v_w (e.g. Poelarends et al. 2008, Ivezić & Elitzur 2010). We are only interested in the radial regime where the wind has reached its asymptotic velocity and the density distribution is $\rho_{gas} = \dot{M}/4\pi v_w r^2$. Thus, one fundamental parameter is the wind density parameter, $\dot{M}/v_w$, which is proportional to both the wind optical depth at any wavelength and the luminosity produced by an outgoing shock wave (see §4.3). We fit the observed spectral energy distributions (SED) of the SN 2008S and NGC 300-OT progenitors using the dusty wind models of DUSTY (Ivezić & Elitzur 1997, Ivezić et al. 1999). Fig. 1 shows the two progenitor SEDs fit as very cool stars ($T_* = 2500$ K) surrounded by dense winds with inner edge dust temperatures of 1500 K.

The models are not unique in terms of stellar temperatures or inner edge dust temperatures, but the stellar luminosity L_* and the density parameter of the wind $\dot{M}/v_w$ are well-defined, as shown in Fig. 2. The SN 2008S progenitor had luminosity $L_* = 10^{4.61\pm0.04} L_\odot$ and requires a wind with $\log(\dot{M}/v_w) = -4.93 \pm 0.12$, where $\log \dot{M} \simeq -3.8 \pm 0.1$ is in $M_\odot$/year and $v_w \simeq 15 \pm 4$ is in km/s. The mass loss and velocity estimates are based on DUSTY's self-consistent wind acceleration models. The NGC 300-OT progenitor had luminosity $L_* = 10^{4.90\pm0.04} L_\odot$ and requires a wind with $\log(\dot{M}/v_w) = -4.26 \pm 0.06$, where $\log \dot{M} \simeq -3.2 \pm 0.1$ is in $M_\odot$/year and $v_w \simeq 12 \pm 3$ is in km/s. The time required for the wind to expand to these radii is consistent with the $\lesssim 10^4$ year limit on the lifetimes of the progenitors in this state (Thompson et al. 2009).

As emphasized by Ivezić & Elitzur (2010), there is a limit to the mass loss rate that can be driven by radiation pressure on dust, which they refer to as the "reddening bound." If these are extreme AGB stars with masses of order $M_* \simeq 9 M_\odot$, the progenitors are near but below this limit for graphitic dust, but above the limit for silicate dusts. This adds further support for graphitic over silicate dusts in these systems (see Prieto et al. 2009, Wesson et al. 2010). The winds of these systems are still extreme, and not those of typical AGB stars with dusty winds (e.g. Matsuura et al. 2009). But we already know that these are very atypical stars, with short lifetimes and only a few such systems per galaxy (Thompson et al. 2009, Khan et al. 2010).

The parameter which best scales our later results is the radius at which the visual optical depth of the progenitor wind is unity, $R(\tau_V = 1)$. The DUSTY model estimates of this radius are shown in Fig. 3, and they can be well-approximated by

$$\begin{aligned} \log R(\tau_V = 1) &= 16.92 + 2.24(\log L_* - 4.61) - a(\log L_* - 4.61)^2 \\ \log R(\tau_V = 1) &= 17.57 + 1.32(\log L_* - 4.90) \end{aligned} \quad (1)$$

for SN 2008S and the NGC 300-OT, respectively. Here, $a = 16$ if $\log L_* < 4.61$ and $a = 0$ if $\log L_* > 4.61$, and the luminosity ranges are $4.51 < \log L_* < 4.79$ (SN 2008S) and $4.78 < \log L_* < 5.03$ (NGC 300-OT). This radius is directly related to the wind density parameter

$$\frac{\dot{M}}{v_w} = \frac{4\pi R(\tau_V = 1)}{\kappa_V} \quad (2)$$

with a visual opacity $\kappa_V = 137$ cm^2/g, as shown in Fig. 2. The wind density depends on both the bulk density of the dust, where we have used $\rho_{bulk} = 2.2$ g/cm^3 for graphitic dust (Ivezić & Elitzur 2010), and the gas-to-

dust ratio, where we are presenting results for DUSTY's default ratio of $r_{gd} = 200$. The density parameter, $\dot{M}/v_w$, mass loss rate $\dot{M}$ and wind velocity v_w scale as $r_{gd}\rho_{bulk}$, $(r_{gd}\rho_{bulk})^{3/4}$ and $(r_{gd}\rho_{bulk})^{-1/4}$, respectively. More importantly, the models of the progenitor's SED directly constrain only $R(\tau_V = 1) \propto \dot{M}\kappa_V/v_w$, so we can increase the gas density of the wind $\dot{M}/v_w \propto r_{gd}$ by reducing the dust opacity per unit mass $\kappa_V \propto r_{gd}^{-1}$, while leaving the dust radiative transfer unchanged and ignoring the problem of accelerating the wind. The default DUSTY value of $r_{gd} = 200$ is larger than the ratio typical of the ISM ($r_{gd} \simeq 100$), and this is generally true of AGB star winds (Ivezić & Elitzur 2010). While we leave the gas-to-dust ratio fixed to this default, it does provide a means of changing the gas density and thus the shock luminosity and X-ray emission we discuss in §4.3 without altering the models for the SEDs.

Most models of these systems have tried to normalize the parameters using a dust photosphere at radius R_{d*} with temperature T_{d*}, where $L_* = 4\pi R_{d*}^2 \sigma T_{d*}^4$ (e.g. Prieto et al. 2008b, Thompson et al. 2009, Botticella et al. 2009, Prieto et al. 2009, Berger et al. 2009, while Wesson et al. (2010) fit dusty radiation transfer models). There is no well-defined mid-IR photosphere, however, because the optical depth varies rapidly with wavelength. In the DUSTY models, the ratios between the visual opacity and those at 5, 7 and 10μm are $\kappa_V/\kappa_5 \simeq 79$, $\kappa_V/\kappa_7 \simeq 138$ and $\kappa_V/\kappa_{10} \simeq 200$, respectively. If we simply estimate where the radius $R(\tau_7 = 1)$ at which the 7μm (chosen to lie close to the peaks of the two SEDs) optical depth is unity, we can illustrate the simple scaling between radius and wavelength-dependent optical depths. The simple $\rho \propto 1/r^2$ model prediction that $R(\tau_7) = R(\tau_V)(\tau_V/\tau_7)(\kappa_7/\kappa_V) = 10^{14.78}$ and $10^{15.42}$ cm for $\tau_7 = \tau_V = 1$ and $\kappa_V/\kappa_7 = 138.5$ agrees well with the DUSTY models, as illustrated in Fig. 3.

3. The Evolution of the Transients

The next step is to characterize the evolution of the transients. Figs. 4 and 5 show snapshots of the evolution of the SEDs of SN 2008S and the NGC 300-OT, and Figs. 6 and 7 show the evolution of the optical, near-IR and mid-IR light curves. The data for SN 2008S comes from Botticella et al. (2009), Smith et al. (2009), Wesson et al. (2010), Prieto et al. (2011) and Hoffman et al. (2011), while that for the NGC 300-OT comes from Bond et al. (2009), Berger et al. (2009), Prieto et al. (2009), Prieto et al. (2010), Ohsawa et al. (2010) and Hoffman et al. (2011). We will model these SEDs with DUSTY, ignoring light travel times ("dust echoes", Wright 1980, Dwek 1983), as these have already been considered in some detail by Wesson et al. (2010), and we are primarily interested in the later time behavior when they are unimportant. This does mean that our very early time models will somewhat mis-characterize the dust properties, where the general sense is to underestimate the radius of the dust and its optical depth. However, on the logarithmic scales in which we are interested, these are minor corrections, and we will incorporate echoes into our light curve models to explore their effects. We can see from Figs. 4 and 5 that the transients, like the progenitors, cannot be well-characterized without mid-IR observations. In fact, in the most plausible models, the NGC 300-OT peaked in the mid-IR rather than the optical. In both cases, as the luminosity drops, the SED shifts from the optical to the mid-IR and the transients again become fully obscured (Prieto et al. 2010, Prieto et al. 2011).

The relevant variables for describing the transients are the (bolometric) luminosity and temperature of

the transient and the characteristic radius and optical depth of any surrounding dust. We first estimated these quantities using DUSTY models of the individual epochs shown in Figs. 4 and 5. DUSTY's structure makes it difficult to produce an evolving series of models to fit the light curves, so we fit the light curves using simpler physical models constrained by both the DUSTY models and the light curves. In these models for the evolution of the light curves, the transients are modeled with a varying luminosity, $L(t)$ and temperature $T(t)$ black body transient, obscured by a time varying dust optical depth $\tau_V(t)$ located at radius $r_d(t)$. The shock velocities were constrained by the estimates of v_s = 1100 and 560 km/s for SN 2008S and the NGC 300-OT from Smith et al. (2010). The luminosity evolution can almost be modeled as an exponential decline plus a constant, $L = L_0 \exp(-t/t_0) + L_1$, and the temperature $T(t)$ can almost be held constant, but this proved to be inadequate for detailed models of the light curves. Thus, we modeled the logarithms of the luminosity, temperature and optical depths as piecewise linear functions. We also included an initial unobserved luminosity spike that heats the dust at radius $r_d(t = 0)$ to a destruction temperature of T_{dest} = 1500 K. The dust emission is then time averaged to include the effects of "dust echoes" in the light curve models. The full details of the model are presented in the Appendix. Obviously, this model has some *ad hoc* features, but it produces remarkably good fits to the light curves given its simplicity, as shown in Figs. 6 and 7. The modest mismatches of the DUSTY and semi-analytic estimates of the dust radii and optical depths illustrate some of the biases created by the approximations.

Fig. 8 summarizes the luminosity evolution of the transients. The luminosities drop exponentially in the early phases and then settle at a nearly constant plateau, given the uncertainties in reconstructing the luminosity with variable wavelength coverage. If we approximate the luminosity as $L = L_0 \exp(-t/t_0) + L_1$, we find $L_0 \simeq 10^{7.3} L_\odot$, $L_1 \simeq 10^{5.8} L_\odot$ and $t_0 \simeq 48$ days for SN 2008S and $L_0 \simeq 10^{7.8} L_\odot$, $L_1 \simeq 10^{5.5} L_\odot$ and $t_0 \simeq 39$ days for the NGC 300-OT. The uncertainties are almost entirely systematic, so we do not report formal statistical uncertainties. Thus, the NGC 300-OT transient was actually brighter, rather than fainter than SN 2008S, and radiated more energy in the transient phase ($E \simeq 3 \times 10^{47}$ ergs for SN 2008S versus $E \simeq 8 \times 10^{47}$ ergs for the NGC 300-OT). Here we have calculated only the contribution from the exponential term. The energy associated with the constant term is unimportant on time scales of t_0, but matches it if the emission continues for 4 and 21 years for SN 2008S and the NGC 300-OT, respectively. SN 2008S has nearly reached this point, while the time scale is much longer for the NGC 300-OT because of its stronger transient and lower plateau luminosity. The inferred peak luminosities, $L_0 \simeq 8 \times 10^{40}$ and 2×10^{41} ergs/sec are comparable to those of low luminosity Type IIP SNe (e.g. Pastorello et al. 2004). In the plateau phase, SN 2008S is brighter than the NGC 300-OT, and both transients remain significantly brighter than their progenitor stars. In both cases, the energetics and luminosities derived from traditional optical approaches are highly misleading – for example, the luminosity history of these transients including the mid-IR emissions is very different from the histories based only on optical observations presented by Smith et al. (2010).

Fig. 9 shows the evolution of the optical depths. Where the progenitors had enormous dust optical depths, the transients at peak had little obscuration, only $\tau_V \simeq 0.3$ for SN 2008S and $\tau_V \simeq 2$ for the NGC 300-OT (Prieto et al. 2008b, Botticella et al. 2009, Bond et al. 2009, Wesson et al. 2010). Note the congruence between the optical depth estimates at peak in Fig. 9 and the optical depth of the progenitor wind outside the

estimate of the initial radius of the dust in Fig. 10. As the transients evolve, the dust optical depth steadily rises, with $\log \tau_V \simeq 1.9 \pm 0.7$ for the final DUSTY epoch in both cases, where the large uncertainties are due to the incomplete wavelength coverage in the final epochs. The optical depth does not, however, initially rise to the total optical depth of the progenitor wind outside the estimated emission radius, but it does appear to steadily approach such optical depths at later times. As the dust destruction radius recedes, the dust appears to reform from the outside inwards, but some time is required before the optical depth returns to the full pre-transient values. The time scale for restoring most of the dust opacity outside the expanding shock appears to be approximately 2-3 years in both systems.

In the DUSTY models, the preferred transient radiation temperatures drop from 7000-8000 K in the first month to 5500-6500 K after 100 days, similar to the evolution in the semi-analytic models. These tend to be somewhat warmer than previous models where the optical temperature was estimated by fitting the emission without a self-consistent model for the dust absorption. At later times, the heavy obscuration makes it impossible to estimate the intrinsic temperature of the transient. As the dust reforms and the characteristic radius of the dust shrinks, the characteristic dust temperature rises with a peak temperature after roughly 8-9 months. This supports the strong near-IR emission in both sources even as the optical emission is collapsing. Fig. 10 shows that the initial transient must destroy the dust out to a radius of order 10^{17} cm, and it then seems to reform from the outside inwards as the dust destruction radius retreats. Eventually the radius of the dust approaches the shock radius and the SED models are consistent with the dust radius starting to expand outwards again.

While there is no ambiguity about the presence of dust near the peak of SN 2008S due to the early-phase mid-IR detections of Wesson et al. (2010), our claim of a significant dust optical depth at the peak of the NGC 300-OT differs strongly from the view of Berger et al. (2009) that there was no dust optical depth near the peak and perhaps weakly with the modest obscuration proposed by Bond et al. (2009). The first argument in Berger et al. (2009) is that their optical/UV SED at 43 days is well-fit by a ~ 4700 K black body with no extinction based on the photometry from z-band to the SWIFT UVW1 (2500Å) band. In Fig. 5 we have extended this wavelength baseline to include the near-IR data from Bond et al. (2009) and shifted to a slightly earlier date (25 May instead of 31 May) in order to include the shorter wavelength SWIFT UVW2 (1900Å) measurement from Berger et al. (2009) with less of a correction based on the evolution of the UVW1 magnitudes. Compared to a cool, 4700 K black body, the SED has both a near-IR and UVW2 excess, which the DUSTY models resolve by using a hotter (~ 9000 K) spectrum with an optical depth of $\tau_V \simeq 2.3 \pm 0.3$. This optical depth is also the amount required to reproduce the Balmer decrement observed by Berger et al. (2009). Bond et al. (2009) interpret the spectra as suggesting that the photosphere has the intrinsic color/temperature of an F star, which then suggests $\tau_V \simeq 1$, but they did not directly fit the SEDs.

Berger et al. (2009) argue against any surviving dust based on the absence of significant Na I D absorption in their spectra. The lack of absorption is remarkable because the total sodium column density of the circumstellar medium is of order $10^{15-16} \tau_V$ cm^{-2}, where $\tau_V \gtrsim 10^2$ is the visual optical depth of the material obscuring the progenitor. Unsaturated Na I D absorption lines mean that all the sodium exterior to the expanding shock has to be photoionized independent of the survival of any dust. The flux required to photoionize a $\rho \propto 1/r^2$ wind from r_{in} to r_{out} scales as $Q = Q_0(1 - r_{in}/r_{out})$ where for pure hydrogen

$Q_0 = \dot{M}^2 \alpha_B / 4\pi v_w^2 m_p^2 r_{in}$, which is very different from the $Q \propto r_{out}^3$ scaling of a uniform density medium (e.g. Fransson 1982). In a wind, once there are enough ionizing photons, $Q \simeq Q_0$, to ionize the inner parts of the wind, virtually no additional ionizing photons are required to ionize the entire wind. For example, at 100 days in the NGC 300-OT, the shock radius of $\sim 10^{14.6}$ cm is well inside the progenitor's dust "photosphere" at $\sim 10^{15.6}$ cm, so the sodium in the dense parts of the wind has to be photoionized. Expanding the sodium Strömgren sphere from the dust "photosphere" to infinity then only requires $\sim 10\%$ more ionizing photons. Moreover, while the transients cannot keep hydrogen and helium fully ionized due to their low radiation temperatures, they are hot enough to produce sodium ionizing photons (see §4.2), thereby allowing hydrogen and helium to recombine while keeping sodium photoionized. This leads to very long sodium recombination times due to the lack of electrons, making it sill easier to keep sodium photoionized. Thus, at the phases of the spectroscopic observations, we expect no Na I D absorption from the wind, and the weak Na I D absorption found by Berger et al. (2009) is due to a small amount of interstellar absorption.

4. A Physical Model for the Transients

All these features of the evolution of the transient can be explained as a consequence of an explosive transient from a red supergiant surrounded by a dense, dusty wind. We assume a wind normalized by the progenitor properties from §2 and shock velocities near the values of v_s = 1100 and 560 km/s proposed by Smith et al. (2010) for SN 2008S and the NGC 300-OT. In §4.1 we consider the implications of the dust radius and optical depths shortly after the peak of the transient, and find that it requires an explosive transient from a red supergiant. In §4.2 we consider recombination, cooling and dust reformation in the progenitor wind following this luminosity peak. In §4.3 we explain the roughly constant late time luminosity as emission from an expanding shock propagating through the dense, progenitor wind. Eventually, the wind column density outside the shock is low enough for the X-rays to be visible, but at early times we expect neither detectable X-ray nor radio emission from the shock. Finally, in §4.4 and §4.5 we discuss the evolution of the optical, near-IR and mid-IR emissions and the potential detectability of surviving progenitor stars.

The X-ray and UV emission produced by an SN shock wave propagating through circumstellar material has been considered extensively (e.g. Chevalier 1982, Fransson 1982, Lundqvist & Fransson 1988, Chugai 1992, Chevalier & Fransson 1994, Chugai & Danziger 1994). Most of these models were developed for normal supernovae with early and long-lived X-ray emission (e.g. SN 1978K, Schlegel et al. 1999 or SN 1980K, Canizares et al. 1982). Our outline of a model for SN 2008S and the NGC 300-OT are simple versions of these earlier models. The resulting expectations only differ from these models because these transients have significantly lower luminosities and shock velocities and are expanding into exceptionally dense, dusty winds.

4.1. Dust Destruction, Shock Breakout and the Progenitor Radius

In addition to showing the estimates for the typical radius of the dust emission, Fig. 10 also shows the radii corresponding to the dust "photosphere" of the progenitor at 7μm, $R(\tau_7 = 1)$, and the radius where the visual optical depth becomes unity, $R(\tau_V = 1)$, as compared to the dust destruction radius predicted by the simple exponential plus plateau models for the bolometric luminosity shown in Fig. 8. As already noted by Botticella et al. (2009), Prieto et al. (2009), Wesson et al. (2010) and Ohsawa et al. (2010), and illustrated by our models in Fig. 10, the surviving dust lies in the un-shocked wind material and so can only have been destroyed radiatively. Moreover, the required dust destruction radii are an order of magnitude larger then the destruction radius predicted from the observed transient luminosities, as also shown in Fig. 10. The observed transients could only destroy the dust out to radii near the mid-IR "photospheres" of the progenitors, which would have left the transients heavily obscured at peak with $\tau_{peak} > 10$ instead of $\tau_{peak} \simeq 1$.

This leads us to the conclusion that the transients must have had short, un-observed, high luminosity spikes, and were thus explosive transients. If τ_{peak} is the visual extinction at the peak of the transient, then we must destroy the dust out to the radius $R_{dest} \simeq \tau_{peak}^{-1} R(\tau_V = 1)$ where $R(\tau_V = 1)$ is the radius in the progenitor wind where the visual optical depth was unity. The luminosity needed to destroy the dust out to radius R_{dest} is

$$L_{peak} \simeq 16\pi\sigma T_{dest}^4 R_{dest}^2 Q_{rat} = 4 \times 10^{10} \tau_{peak}^{-2} \left(\frac{Q_{rat}^{1/4} T_{dest}}{1500 \text{ K}} \right)^4 \left(\frac{R(\tau_V = 1)}{10^{17} \text{ cm}} \right)^2 L_\odot, \quad (3)$$

where $T_{dest} \simeq 1500$ K is the dust destruction temperature and $Q_{rat} = Q(T_{dest})/Q(T_{peak})$ is the ratio of the Planck-averaged absorption efficiencies at the temperatures T_{peak} of the break out radiation and T_{dest} (e.g. Dwek 1985, Draine & Lee 1984). Q_{rat} depends on grain size because the smaller grains reach higher temperatures for a given radiation field, so for a more accurate estimate of the required luminosities we determined the fraction of the dust destroyed for a Mathis et al. (1977) distribution of Draine & Lee (1984) graphitic dust with the $0.005 < a < 0.25\mu$m size distribution used by DUSTY. A transient peak with luminosity L_{peak} and radiation temperature $T_{peak} = 50000$ K destroys 50% of the dust opacity to radius

$$R_{d50} \simeq 6 \times 10^{16} \left(\frac{L_{peak}}{10^{10} L_\odot} \right)^{1/2} \left(\frac{T_{dest}}{1500} \right)^{-5/4} \text{ cm} \quad (4)$$

and 90% of the dust opacity to $R_{d90} \simeq R_{d50}/2$. Since we require $R_{d50} \simeq R(\tau_V = 1)/\tau_{peak} \simeq 10^{17}$ cm, we must have

$$L_{peak,50} \simeq 3 \times 10^{10} L_\odot \left(\frac{R(\tau_V = 1)}{\tau_{peak} 10^{17} \text{ cm}} \right)^2 \left(\frac{T_{dest}}{1500 \text{ K}} \right)^{2.5} L_\odot \quad (5)$$

with the luminosity $L_{peak,90}$ needed to destroy 90% of the opacity being roughly 4 times higher. *Such a high peak luminosity can only be explained by the luminosity produced from a shock breaking out of the stellar photosphere, which in turn requires that these were explosive transients rather than some form of radiation pressure driven eruption.*

Producing such a high luminosity with a shock breakout also implies that the progenitor stars were cold, red supergiants. We show this following the approximate breakout model of Ofek et al. (2010) (following

Falk & Arnett 1977, Waxman et al. 2007). The shock breaks out when the radiative diffusion time scale matches the expansion time scale, $t_{diff} = \kappa_T \rho_s r_s^2/c = t_{exp} = r_s/v_s$, where $\kappa_T \simeq 0.4$ cm^2/g is the Thomson opacity. This determines the density ρ_s of the breakout region in terms of the break out radius r_s,

$$\rho_s = \frac{c}{v_s \kappa_T r_s}. \tag{6}$$

The post-shock region is radiation dominated, so the radiative energy density has to match the energy density of the shock, $aT_s^4 = (7/2)\rho_s v_s^2$, where we have assumed the density compression for $\Gamma = 4/3$. Thus,

$$\sigma T_s^4 = \frac{7}{8}\frac{v_s c^2}{\kappa_T r_s}. \tag{7}$$

By setting the break-out luminosity $4\pi\sigma T_s^4 r_s^2 f = L_{peak,50}$, we find that the radius is

$$r_s \simeq 5 \times 10^{13} \left(\frac{R(\tau_V = 1)}{\tau_{peak} 10^{17}\mathrm{cm}}\right)^2 \left(\frac{T_{dest}}{1500\ \mathrm{K}}\right)^{5/2} \left(\frac{1000\ \mathrm{km/s}}{f v_s}\right)\ \mathrm{cm}. \tag{8}$$

This is relatively crude estimate, so we have introduced the dimensionless factor f to monitor the effects of the approximation on other estimates. For example, $f = 0.5$ if we require $L_{peak,90}$ instead of $L_{peak,50}$. If we interpret this as the shock breaking out of the wind, then the wind density parameter must be

$$\frac{\dot{M}}{v_w} = \frac{4\pi c r_s}{v_s \kappa_T} \simeq= 10^{-3.2} \left(\frac{R(\tau_V = 1)}{\tau_{peak} 10^{17}\ \mathrm{cm}}\right)^2 \left(\frac{T_{dest}}{1500\ \mathrm{K}}\right)^{5/2} \left(\frac{1000\ \mathrm{km/s}}{f v_s}\right)^2 \frac{M_\odot/\mathrm{year}}{\mathrm{km/s}}, \tag{9}$$

which is an order of magnitude larger than the wind densities inferred from the progenitor properties (Fig. 2). Thus, the shock breakout radius must correspond to the stellar radius $R_* \simeq r_s$. This implies a stellar temperature of

$$T_* = \left(\frac{L_*}{4\pi\sigma R_*^2}\right)^{1/4} \simeq 4000 \left(\frac{L_*}{10^5 L_\odot}\right)^{1/4} \left(\frac{\tau_{peak} 10^{17}\mathrm{cm}}{R(\tau_V = 1)}\right) \left(\frac{1500\ \mathrm{K}}{T_{dest}}\right)^{5/4} \left(\frac{f v_s}{1000\ \mathrm{km/s}}\right)^{1/2}\ \mathrm{K}. \tag{10}$$

For our nominal estimates of the progenitor luminosities and wind properties from §2 and the optical depths at peak from §3, this yields stellar temperatures of order 1400 K with formal uncertainties of order 30%, but the estimate is really dominated by systematic uncertainties in the models and dust destruction physics – temperature is a variable where logarithmic accuracy is not really adequate. Nonetheless, the estimate is far more consistent with a cool, red supergiant as the progenitor, an EAGB star, than with a hotter, bluer star. The break out luminosity increases with the size of the star, $L_s \propto r_s$, because the larger surface area ($\propto r_s^2$) matters more than the lower shock temperature ($T_s^4 \propto 1/r_s$, Eqn. 7). The duration of the break out peak is of order the light crossing time $r_s/c \sim 10^4$ sec or less, so the energy released in the peak is less than that of the observed transient.

4.2. Recombination, Cooling and Dust Reformation

The transient models from §3 appear to show that (1) the dust optical depth rebuilds from the outside in, (2) that some optical depth returns quickly, but (3) that it takes several years for the optical depth to

rebuild to levels close to that of the progenitor wind. Sadly we lack the continuous, detailed monitoring of the mid-IR spectral energy distributions that would have allowed a careful exploration of this process. In this section we outline some of the relevant physical issues and Fig. 11 outlines our model for the process

The temperature of the shock break out radiation is high, $T_s \sim 50000$ K (Eqn. 7), so the wind is photoionized by the break out radiation. For pure hydrogen, the minimum ionizing flux needed to maintain the ionization is

$$Q_0 = \frac{4\pi\alpha_B R(\tau_V = 1)^2}{R m_p^2 \kappa_V^2} \simeq 2 \times 10^{49} \left(\frac{\alpha_B}{10^{-13}\ \mathrm{cm^3/s}}\right) \left(\frac{140\ \mathrm{cm^2/g}}{\kappa_V}\right)^2 \left(\frac{R(\tau_V = 1)}{10^{17}\mathrm{cm}}\right) \left(\frac{R(\tau_V = 1)}{10R}\right)\ \mathrm{s^{-1}} \quad (11)$$

which cannot be supplied by the transients even at their observed peaks (low luminosity, low temperature, and $R(\tau_V = 1)/R \sim 10^3$). We scale this and the subsequent expressions to the radius $R = 10^{-1}R(\tau_V = 1) \simeq 10^{16}$ cm, roughly corresponding to the shock radius at the present time (~ 3 years at 1000 km/s). Thus, the wind recombines on time scales (for hydrogen) of

$$t_R = \frac{\mu m_p}{\alpha_B \rho_w} = \frac{\mu m_p R(\tau_V = 1)\kappa_V}{\alpha_B} \left(\frac{R}{R(\tau_V = 1)}\right)^2 \simeq 0.43 \left(\frac{R(\tau_V = 1)}{10^{17}\mathrm{cm}}\right) \left(\frac{10^{-13}\mathrm{cm^3/s}}{\alpha_B}\right) \left(\frac{10R}{R(\tau_V = 1)}\right)^2 \text{ years} \quad (12)$$

that are very short in the interior and only become relatively long as you approach $R(\tau_V = 1)$, as shown in Fig. 11. While the transients cannot keep hydrogen and helium in the wind fully ionized due to their low temperatures, they have no difficulty keeping sodium photoionized, as discussed in §3. At late times, as we discuss in §4.3, the source of the luminosity is non-thermal emission from a shock, and ultimately this should reionize the wind because the required number of ionizing photons steadily diminishes.

Then as the gas cools, the dust can reform. The cooling time scale is of order

$$t_{cool} = \frac{3kT\mu m_p \kappa_V r^2}{2\Lambda R(\tau_V = 1)} \simeq 0.089 \left(\frac{T}{10^4\ \mathrm{K}}\right) \left(\frac{10^{-25}\ \mathrm{ergs\ cm^3/s}}{\Lambda}\right) \left(\frac{R(\tau_V = 1)}{10^{17}\mathrm{cm}}\right) \left(\frac{10R}{R(\tau_V = 1)}\right)^2 \text{ years} \quad (13)$$

where a cooling rate of $\Lambda \simeq 10^{-25}$ ergs cm^3/s is approximately correct for $10^3 < T < 10^4$ K (e.g. Schure et al. 2009). Thus, the gas also cools rapidly after the peak, with the cooling radius being only slightly smaller than the recombination radius in Fig. 11.

Once the temperature is low enough, $T \lesssim T_{dest}$ either the dust begins to form anew following a burst of nucleation in the now supersaturated vapor or any residual grains can begin to grow. Given a steadily declining temperature, nucleation is not a bottleneck, although the radius for inhibiting dust formation is larger than the dust destruction radius because less flux is needed to destroy the smallest grains. For a 7000 K transient and $T_{dest} = 1500$ K, graphitic dust can begin to form outside the radius

$$R_{form} \simeq 10^{15.9} \left(\frac{L}{10^8 L_\odot}\right)^{1/2}\ \mathrm{cm}, \quad (14)$$

estimated from the heating of the smallest grains. We used this estimate of the destruction radius in Fig. 10 to illustrate where dust can begin to reform. For both transients, R_{form} is outside the shock radius only for

the first ~ 100 days, as shown in Fig. 11 based on the exponential plus constant luminosity models for the transients from §3. For comparison, Fig. 11 also shows the radius at which 50% of the dust opacity will survive a $L_{peak} = 4 \times 10^{10} L_{\odot}$ break out shock based on Eqn. 5.

The bottleneck for reforming the dust is the growth rate of the particles after nucleation, where the time scale to grow a (spherical) grain of radius a by adding monomers assuming a sticking fraction of unity is of order

$$t_{grow} \simeq \frac{4\rho_{bulk} a}{v_c X_c \rho} \simeq 19 \left(\frac{a}{0.1\mu\mathrm{m}}\right) \left(\frac{0.02}{X_c}\right) \left(\frac{R(\tau_V = 1)}{10^{17}\mathrm{cm}}\right) \left(\frac{10R}{R(\tau_V = 1)}\right)^2 \text{ years} \quad (15)$$

where $v_c \simeq v_w \simeq 10$ km/s is the collision velocity, and X_c is the carbon mass fraction in the wind (we have used a relatively high value appropriate for a carbon rich EAGB wind (Abia & Isern 2000)). If the particles are growing by coagulation rather than monomer accretion, the growth rates are a four times faster, but significantly shorter growth times could only come from incorporating significant numbers of the far more abundant hydrogen atoms, having a reduced dimensionality (e.g. sheets) or density, or starting from more and larger surviving particles at larger radii. In practice, the latter effect is certainly present, so Eqn. 15 does exaggerate the difficulty of reforming dust at larger radii. We should also note that there is no need to fully repopulate the $0.005 < a < 0.25\mu$m size range of the standard DUSTY Mathis et al. (1977) models to recover most of the opacity. DUSTY models using distributions with maximum grain sizes of 0.01, 0.025, 0.05 or 0.1μm instead of 0.25μm have visual opacities smaller only by factors of 3.4, 3.4, 2.9 and 1.6, respectively, consistent with the rapid return of a significant fraction of the pre-transient opacity followed by a slower rise towards the total pre-transient opacity.

Fig. 11 illustrates the cycle of dust formation for SN 2008S. Assuming growth begins after both recombination is completed and the radiative heating is sufficiently low, dust begins to reform at an intermediate radius where the formation time scale is relatively long. However, since the cooling and growth time scales are significantly shorter at smaller radii, the optical-depth weighted radius of the dust will rapidly shrink, roughly tracking R_{form}, until it reaches the expanding radius of the shock. Our models essentially represent the evolution of this optical-depth weighted radius. A variant of the models where we used two shells, one at large radius to represent the dust surviving the explosion, and one expanding with the shock, could not reproduce the light curves as well. We attempt an explicit model of the evolution of the optical depth in Fig. 12. In this model, the dust begins to reform at each radius after the longer of either the recombination time (Eqn. 12) or the time needed to lie outside the region radiatively heated to T_{dest} (Eqn. 14). The maximum particle size a_{max} is then determined from Eqn. 15, and the opacity is found by the scaling of the DUSTY model opacities with a_{max}. Qualitatively this reproduces the behavior of the optical depth in the models, which are also shown in Fig. 11. Quantitatively, the optical depth rises too quickly and is somewhat low at the time of our last SED model. The early time differences could be due to oversimplifying the temperature of the dust at smaller radii where there may be additional heating and destruction mechanisms associated with the ionizing radiation from the expanding shock front (see §4.3). Overall, however, the physical characteristics of the winds are broadly consistent with reforming the necessary amounts of dust.

4.3. X-ray Emission from the Shocks Powers the Late-Time Light Curves

Even after almost three years, these sources are still an order of magnitude more luminous than their progenitors, and the present emission is most likely due to shock heating the dense wind. For a shock wave propagating outward at velocity $v_s >> v_w$, the shock releases energy (e.g. Chevalier 1982, Fransson 1982, Chugai 1992, Chugai & Danziger 1994, Chevalier & Fransson 1994)

$$L_S \simeq \frac{\dot{M}}{2}\frac{v_s^3}{v_w} = \frac{2\pi R(\tau_V = 1)v_s^3}{\kappa_V} = 1.2 \times 10^6 \left(\frac{v_s}{1000\text{km/s}}\right)^3 \left(\frac{R(\tau_V = 1)}{10^{17}\text{ cm}}\right) \left(\frac{140\text{ cm}^2/\text{g}}{\kappa_V}\right) L_\odot \qquad (16)$$

although this energy can be lost due to expansion rather than radiated. In detail, there is both a forward and a reverse shock, separated by a contact discontinuity. Models of X-ray emission for typical SN focus on the reverse shock because of its lower temperature. Here, the low velocities make the forward shock a source of very soft, readily absorbed emission as well. Exactly what should be used for v_s is unclear, since the line widths in normal Type IIn are not believed to be representative of the true shock velocity, but as with the light curve models in §3 we will scale results based on the FWHM estimates from Smith et al. (2010) of v_s = 1100 km/s and 560 km/s for SN 2008S and the NGC 300-OT, respectively. Because of the low shock velocities, the post-shock temperatures are low

$$E_s = \frac{3\mu}{16} m_p v_s^2 = 1.2 \left(\frac{v_s}{1000\text{km/s}}\right)^2 \text{ keV} \qquad (17)$$

for a mean molecular weight $\mu = 0.6$. The optical depth of the swept up wind is the same as that of the wind exterior to the shock for the same opacity, so the swept up wind material quickly becomes Thomson optically thin,

$$\tau_T \simeq \frac{R(\tau_V = 1)}{R}\frac{\kappa_T}{\kappa_V} \simeq 0.09 \left(\frac{R(\tau_V = 1)}{10^{17}\text{ cm}}\right) \left(\frac{1000\text{ km/s}}{v_s}\right) \left(\frac{\text{year}}{t}\right). \qquad (18)$$

The low Thomson optical depth of the wind essentially corresponds to the conclusion in §4.1 that the wind density is too low to be the source of the shock breakout luminosity. Typical models of these shocks consider cooling by adiabatic expansion, Compton cooling and free-free emission, but generally consider much faster shocks ($v_s \sim 10^4$ km/s) in less dense winds, finding that the early-time cooling is dominated by Compton cooling. In these systems, free-free emission dominates over Compton cooling, with a cooling rate of order $\Lambda = A_0 n^2 (T/T_0)^{1/2}$ for T_0 = 1 keV $\simeq 10^7$ K and $A_0 \simeq 2 \times 10^{-24}$ ergs cm^3/s (e.g. Rybicki & Lightman 1979), so the ratio of the cooling time, $t_{cool} = 3nkT_s/2\Lambda$, to the expansion time, $t_{exp} = R/v_s$, is

$$\frac{t_{cool}}{t_{exp}} \simeq 0.5 \left(\frac{v_s}{1000\text{ km/s}}\right)^2 \left(\frac{\kappa_V}{140\text{ cm}^2/\text{g}}\right) \left(\frac{4}{C_{comp}}\right) \left(\frac{10R}{R(\tau_V = 1)}\right) \qquad (19)$$

where $C_{comp} > (\Gamma+1)/(\Gamma-1) = 4$ is the ratio of the post-shock density to the pre-shock density. Thus, the shock energy will be efficiently radiated as soft X-rays until the shock radius approaches $R(\tau_V = 1)$.

Unlike typical SN, the combination of high wind densities and a very soft X-ray spectrum mean that the X-ray emission is fully absorbed by the unshocked wind material and radiated in the mid-IR by the reformed dust while the wind is optically thick. Following Draine & Woods (1991), we model the (bound-free) X-ray

opacity of the wind as

$$\begin{aligned} \kappa_H(E) &= 17(E/\mathrm{keV})^{-3}\ \mathrm{cm}^2/\mathrm{g} \\ \kappa_Z(E) &= 85\left(1+(E/\mathrm{keV})^{2.5}\right)^{-1}\ \mathrm{cm}^2/\mathrm{g} \end{aligned} \tag{20}$$

from neutral hydrogen/helium and heavier elements, respectively. This implies X-ray optical depths of

$$\begin{aligned} \tau_H(E) &= 1.2\left(\frac{140\mathrm{cm}^2/\mathrm{g}}{\kappa_V}\right)\left(\frac{R(\tau_V=1)}{10R}\right)\left(\frac{E}{\mathrm{keV}}\right)^{-3} \\ \tau_Z(E) &= 6.1\left(\frac{140\mathrm{cm}^2/\mathrm{g}}{\kappa_V}\right)\left(\frac{R(\tau_V=1)}{10R}\right)\frac{1}{1+(E/\mathrm{keV})^{2.5}}. \end{aligned} \tag{21}$$

from radius R to infinity. The corrections for the material outside the recombination radius (Eqn. 12) are not important until very late. The free-free emission spectrum is

$$F_\nu \propto g(E/E_0)\exp(-E/E_0) \tag{22}$$

where $g(x)$ is the Gaunt factor. For an X-ray temperature of E_0 = 1 keV, the fraction of the X-ray energy escaping the wind for $R/R(\tau_V = 1)$ = 0.01, 0.1, and 1 is only 0.2%, 5%, and 27%, with mean energies of 4.8, 2.6 and 1.5 keV. Slightly more escapes for SN 2008S ($E_0 \simeq 1.2$ keV) and quite a bit less escapes the NGC 300-OT ($E_0 \simeq 0.4$ keV). While soft X-ray absorption from SN shocks has been discussed in the context of normal SN models (e.g. Fransson 1982), the overall spectrum is assumed to be much harder (because v_s is larger), so only small fractions of the total luminosity are absorbed.

We can approximate the expected X-ray emission as

$$L_X \simeq L_S\frac{1-f_{abs}}{1+t_{exp}/t_{cool}} \tag{23}$$

where L_S is the shock luminosity from Eqn. 16, $1-f_{abs}$ is the unabsorbed fraction estimated by combining the wind model, the X-ray optical depths in Eqn. 22 and the shock energies from Eqn. 17, and the denominator approximates the balance between radiative and expansion losses from Eqn. 19. When the cooling time is short, all the energy is radiated, while when it is long, only the fraction t_{cool}/t_{exp} is radiated and the remainder is lost to adiabatic expansion. The evolutions of the expected X-ray luminosity and the mean photon energy for the two systems are shown in Fig. 13. Without absorption, both systems should be bright X-ray sources. With absorption, however, they are relative faint, hard X-ray sources in the early phases, and it is not at all surprising that they were not detected in the early SWIFT observations (Botticella et al. 2009, Berger et al. 2009). While SN 2008S has not been reobserved, the NGC 300-OT was reobserved after roughly two years by both SWIFT (Berger & Chornock 2010) and Chandra (CXO observation ID 12238/PI: Williams). Fig. 13 indicates the count rates at which these various observations would detect 3 source photons, where we estimated the count rates using the Chandra/SWIFT exposure time calculators and absorbed thermal bremsstrahlung models based on the gas column densities in our nominal wind models for the two sources. Neither source should have been detectable in any of the observations to date. SN 2008S should now be relatively easy to detect, with count rates of order 10^{-3}/sec, but has not been observed, while

the NGC 300-OT is essentially undetectable – it is less luminous, softer, and more heavily obscured. Bear in mind, however, that at fixed shock luminosity, the detectability of the X-ray emission depends exponentially on the shock velocity because the X-ray optical depth of the wind scales as L_s/v_s^4 (three powers of v_s from the shock luminosity, Eqn. 16, and one power because of the slower expansion through the wind), and the typical energy scales as v_s^2 (Eqn. 17). Small reductions in v_s dramatically increase the overall absorption.

Such shocks are also expected to produce radio emission, which has not been observed (Chandra & Soderberg 2008, Berger et al. 2009), and this is also used as evidence against an explosive transient. In fact, no early time radio emission is likely to escape the wind exterior to the shock because absorbing the X-ray emission will create an ionized layer in the unshocked wind exterior to the shock. If this ionized layer has a thickness ΔR, and electron temperature $T_e \simeq 10^4$ K, then the free-free optical depth of the layer is

$$\tau_\nu \sim 2000 \nu_{GHz}^{-2.1} \left(\frac{10^4 \text{ K}}{T_e}\right)^{1.35} \left(\frac{10\Delta R}{R}\right) \left(\frac{10^{17} \text{ cm}}{R(\tau_V = 1)}\right) \left(\frac{R(\tau_V = 1)}{10R}\right)^3 \quad (24)$$

and these systems will be very optically thick to GHz radio emission in their early phases and should not have been detectable. The time scale for the optical depth to fall to $\tau_\nu = 1$ is

$$t_\nu \sim 40 \nu_{GHz}^{-0.7} \left(\frac{R(\tau_V = 1)}{10^{17} \text{ cm}}\right)^{2/3} \left(\frac{10\Delta R}{R}\right)^{1/3} \left(\frac{10^4 \text{ K}}{T_e}\right)^{0.45} \left(\frac{1000 \text{ km/s}}{v_s}\right) \text{ years} \quad (25)$$

ignoring any other potential source of opacity at these wavelengths. Thus, at late times these systems may be detectable in the radio. More generally radio emission from such high density winds or from shocked, massive shells of material will be very different from the significantly lower regimes of circumstellar densities that are usually considered for radio supernovae (e.g. Chevalier et al. 2006).

4.4. Mid-IR, near-IR and Optical Emission

The current mid-IR emission is simply the absorbed X-ray flux combined with any emission from dust heated and destroyed by the shock. The absorbed X-ray emission leads to a mid-IR luminosity of

$$L_{IR} \simeq L_S \frac{f_{abs}}{1 + t_{exp}/t_{cool}}. \quad (26)$$

which is simply the absorbed counterpart to Eqn. 23, as long as the dust optical depth remains high. Here we are ignoring the extra emission from dust directly heated by the shock, which typically radiates $\sim 10\%$ of the shock luminosity (Draine 1981). The dust temperature is simply determined by the available luminosity, since emission by the dust is the only means of radiating the absorbed energy. Thus, the dust temperature must be or order

$$T_d \simeq \left(\frac{L_{IR}}{16\pi\sigma r_d^2}\right)^{1/4} = 440 \left(\frac{L_{IR}}{10^6 L_\odot}\right)^{1/4} \left(\frac{1000 \text{ km/s}}{v_s}\right)^{1/2} \left(\frac{1000 \text{ days}}{t}\right)^{1/2} \text{ K}. \quad (27)$$

where r_d is the dust radius. Driven by the declining luminosity and the increasing dust radius, the mid-IR emission slowly declines and shifts to longer wavelengths, as we see in Figs. 6 and 7. This phase lasts until

the shock expands to the point that the optical depth of the reformed dust begins to clear. If all the dust has reformed, it takes

$$t(\tau_\lambda) = \frac{R(\tau_V = 1)}{v_s \tau_\lambda} \frac{\kappa_\lambda}{\kappa_V} = 31 \left(\frac{R(\tau_V = 1)}{10^{17} \text{ cm}} \right) \left(\frac{1000 \text{ km/s}}{v_s} \right) \frac{\kappa_\lambda}{\kappa_V} \frac{1}{\tau_\lambda} \text{ years} \quad (28)$$

for the optical depth down to the shock to be τ_λ. In Figs. 6 and 7 this leads to the sequential recovery of the near-IR and then the optical fluxes, with the present period being the phase where the absorption is worst. In these models, the near-IR fluxes should begin to recover in the immediate future.

Unfortunately, the late time details of the light curves in Figs. 6 and 7 are incorrect because the models simply continue to assign the transient a black body SED of fixed temperature. This approximation is adequate when the optical emission is dominated by the transient rather than the shock or when the emission is all absorbed and re-radiated in the mid-IR, but it is not correct when the dust opacities become low enough for the line emission from the shock to escape. The SED of the shock will be a complex line spectrum (e.g. Fesen & Matonick 1994 for SN 1980K) extending from the UV into the mid-IR (e.g. Allen et al. 2008) rather than a black body. The Allen et al. (2008) shock models do not reach the wind densities needed for these systems, but to the extent we can extrapolate from the highest density models in their survey, the dominant emission is in the UV (Lyα), followed by the optical (Hα) and mid-IR, with relatively little emission in the near-IR. Hence, the extrapolations shown in our light curve models are probably over-estimating the recovery in the near-IR. Fig. 14 shows the effect on the light curve of SN 2008S if we model the shock emission using the emission lines and line ratios of the highest density ($n = 10^3$ cm^{-3}), solar metallicity, $v_s = 1000$ km/s models from Allen et al. (2008). The true density is much higher, and so the actual line ratios will be strongly affected by the collisional de-excitation effects that limited their survey of shock emission spectra to $n \leq 10^3$, but it illustrates the potential differences from the model used in Fig. 6. As a result, these shock models have no significant recovery of the near-IR flux as the optical depth drops.

4.5. Did the Stars Survive?

Because the shock luminosity is significantly greater than that of the progenitor, we can only indirectly constrain the existence of a surviving star. One probe of this question is the mass of the ejecta. Using the expansion velocities of $v_s = 1100$ and 560 km/s from Smith et al. (2010) for the transients, and assuming the radiated energy estimates from §3 are fraction f of the kinetic energy, the ejected masses are of order $M_e \sim 0.02 f^{-1} M_\odot$ and $0.25 f^{-1} M_\odot$ for SN 2008S and the NGC 300-OT transient. Since destroying the dust required an explosive transient, we would expect $f \sim 0.01$ as is typical of supernovae rather than $f \sim 1$ similar to η Carinae (e.g. Smith et al. 2010), but this argument is too crude to determine the survival of the star. The roughly constant shock luminosity means that the ejected mass must significantly exceed the swept up wind mass, so $M_e \gtrsim 3\dot{M} v_s t / v_w$, which after $t \simeq 3$ years corresponds to $M_e \gtrsim 0.05 M_\odot$ and $0.25 M_\odot$ for our standard parameters, weakly requiring $f \gtrsim 1$. Unfortunately, the time scales for estimating M_e from the evolution of the transients are long.

This leaves the problem of directly detecting a surviving star. As the shock expands, the pre-existing

wind will stop cloaking the progenitor and the shock luminosity will fade due to the decreasing radiative efficiency and will likely be dominated by X-ray and line emissions that are not characteristic of the progenitor. Fig. 14 shows the effect of including the SN 2008S progenitor as a $T_* = 3000$ K black body in the shock model for the late-time emissions. This assumes that no dust has formed in or behind the shock but includes the obscuration from the wind exterior to the shock. Obviously, if dust forms either near the contact discontinuity between the ejecta and the wind or in the ejecta, there is easily enough material to fully cloak the star. Moreover, the luminosity of the shell plus any surviving star is insufficient to maintain a temperature above the dust destruction temperature in the region interior to the reverse shock.

5. Summary

The available data for the SN 2008S and the NGC 300-OT are consistent with a relatively simple, self-consistent physical picture of the systems. The progenitor stars are luminous, cool, red supergiants, most likely EAGB stars based on their positions in mid-IR CMDs in a short-lived state with very high mass loss rates (Thompson et al. 2009, Khan et al. 2010). The very dense winds form so much dust that they are optically thick in the mid-IR with dust photospheres on scales of a few 10^{15} cm and optical photospheres near 10^{17} cm. They are best modeled with graphitic dusts (Prieto et al. 2009, Wesson et al. 2010), and the radiatively driven dusty wind models of Ivezić & Elitzur (2010) can produce such winds at the $\sim 9M_{\odot}$ mass scale of EAGB stars assuming graphitic, but not silicate, dusts.

Both stars then underwent an explosive transient with a short duration, very high luminosity shock breakout spike. This unobserved luminosity peak is necessary because the observed luminosity peaks are not nearly bright enough to destroy dust to the distances needed to have the transient peaks little extincted. We know from early-time mid-IR observations of Wesson et al. (2010) that SN 2008S had a modest surviving dust optical depth, and our models of the early-time UV through near-IR SED of the NGC 300-OT from Berger et al. (2009) and Bond et al. (2009) imply a surviving visual optical depth of a few, which is consistent with the Balmer decrement observed by Berger et al. (2009). Berger et al. (2009) argue that the weak Na I D absorption in spectra of the NGC 300-OT imply no surviving dust, but we argue that sodium must remain photoionized independent of any surviving dust and would be uncorrelated with any surviving dust if present. Similarly, the dense circumstellar wind is initially opaque to X-rays and requires very little ionization to be opaque to radio emission, so the failure to detect the systems at both X-ray and radio wavelengths at early-times is also a natural consequence of the progenitor properties even for an explosive transient. The stellar radius required by the shock break out model also requires a large, cool star, again consistent with the EAGB picture for the progenitor stars.

The evolution of the transient SEDs with time is largely controlled by the reformation of the dust in the progenitor wind outside the expanding transient shock wave. The average dust radius appears to move inwards from near the original optical photosphere as the dust destruction radius shrinks. The dust radius then appears to begin to expand again to track the estimated radius of the shock wave passing through the wind, although the evidence for this is less striking than the initial shrinking of the dust radius. Initially, the

optical depth is significantly less than that of the progenitor wind outside the same radius, but the fraction of the dust that reforms steadily rises, with most of the dust having reformed after about 2-3 years. The dust radius shrinks faster than the transient luminosity drops, so that the dust temperature peaks 8–9 months after the transient peak, and this rising dust temperature balances the falling luminosity to produce relatively extended, slowly varying near-IR light curves. The optical fluxes drop very rapidly from the combination of the dropping luminosity and the rising optical depths. Although the luminosity eventually becomes roughly constant, the optical depth continues to rise and the systems fade in the near-IR. At present, neither system is detected at optical wavelengths (Prieto et al. 2010, Prieto et al. 2011), and SN 2008S is at best marginally detectable in the near-IR even with HST (Prieto et al. 2011). In the mid-IR, however, both systems are easily detected with significantly higher temperatures and luminosities than the progenitor stars.

The average dust radius in our models is an optical depth weighted mean radius, and the true evolution is more complicated. Models with a surviving shell of dust and a shell of forming at the the expanding shock radius work poorly – successful models require dust reforming in the exterior wind and are incompatible with a shell ejection scenario, just as was true of the pre-transient mid-IR variability. The optical depth of the reformed dust is dominated by the smallest radius at which dust can reform because the particle growth rates are proportional to density, so the effective dust radius shrinks rapidly, tracking the decaying luminosity with a delay, until it encounters the expanding shock. The simple model of a smoothly shrinking dust radius elides over a gap at 10^{16} to 10^{17} cm, between the surviving and reforming dust, where the particle growth times are too long for rapid reformation. This pattern of a receding dust radius is also reported for the Type IIP SN 2007it (Andrews et al. 2011) and SN 2007od (Andrews et al. 2010), although the implied optical depths are much lower. Re-forming CSM dust sufficiently quickly requires the high densities of slow, high $\dot{M}$ winds or massive shells of ejecta. In most systems, only the normal scenarios are relevant because the particle growth rates are too slow: dust must either survive the explosion, form in cooled shocked CSM near the contact discontinuity or form in the un-reverse-shocked ejecta. The high CSM densities that allow rapid dust reformation are yet another new (or odd) property of these transients.

The present day, roughly constant luminosities closely match the luminosity expected from expanding shocks heating the progenitor winds. The shocks are Thomson optically thin but radiatively efficient, leading to high $\sim 10^{5.5} L_{\odot}$, soft (0.5-1.0 keV) X-ray luminosities. Soft X-ray opacities are, however, not very different from dust opacities, so the dense progenitor winds simply absorb the shock luminosity and the energy is ultimately radiated in the mid-IR, leading to the present-day spectral energy distributions. Neither source should have been detectable in the X-ray observations of these systems to date, despite having intrinsic X-ray luminosities of order 10^{39} ergs/s. As the shock moves outward, the X-rays begin to escape and should show a spectrum with strong absorption at 0.5-2.0 keV that will be a powerful probe of the wind column density. SN 2008S, which has a lower density progenitor wind and a faster shock velocity, should now be relatively easy to detect as an X-ray source, while the NGC 300-OT should still be very difficult to detect because of its higher density wind and slower shock velocity. Slower shock velocities reduce the X-ray detectability partly because the slower shock expansion rate slows the drop in the exterior wind column density and partly because the lower shock temperature leads to a softer more easily absorbed X-ray spectrum. The detectability does, however, depend exponentially on the assumed shock velocity. The

peak X-ray emission is a balance between the diminishing absorption column density and the diminishing radiative efficiency of the shock, peaking on time scales of order 10 years for SN 2008S and much later for the more slowly evolving, more heavily obscured NGC 300-OT. Absorbing the X-ray emission will produce an ionized region in the unshocked wind just outside the shock, and the resulting free-free opacity will also block any GHz radio emission produced by the shock for an extended period of time. Thus, the failure to detect early-time radio emission is also expected.

The balance between dust reformation and shock expansion means that the visual optical depth to the shock peaked after roughly 2-3 years and should now be dropping linearly with time. The mid-IR luminosity should steadily diminish, because there is less absorption, and shift to longer wavelengths, because the larger dust radius and diminished luminosity lead to lower dust temperatures. It may be difficult to cleanly separate these trends with only 3.6 and 4.5μm warm Spitzer observations. Near-IR observations will shortly be able to penetrate to the shock front, although the visual optical depth to the shock front will not approach unity for over a decade. The optical/near-IR emission from the shock region should be a combination of free-free emission, line emission driven by X-ray absorption and shock heated dust. In the evolution to date, the luminosity was dominated by the shock emission while the dust optical depths are high enough to allow us to ignore these details, which will not be true of these later phases. Unfortunately, until the luminosity fades or we can penetrate the dust, it is impossible to determine the fate of the progenitor star.

The author would like to thank J.F. Beacom, J.A. Johnson, M. Pinsonneault, J.-L. Prieto, R. Pogge, K. Sellgren, K.Z. Stanek, D. Szczygiel, T.A Thompson and B.E. Wyslouzil for extensive discussions. CSK is supported by NSF grant AST-0908816. This research has made use of the NASA/IPAC Extragalactic Database (NED) which is operated by the Jet Propulsion Laboratory, California Institute of Technology, under contract with the National Aeronautics and Space Administration.

A. Light Curve Fits

Here we spell out the details of the light curve fitting procedure. We specify the luminosity and optical depth on a grid of times t_i with $i = 1 \cdots N$ and $t_1 \equiv 0$. The transient luminosity $L_i = L(t_i)$ and temperature $T_i(t_i)$ are determined at each grid point, and the value at time t is found by linearly interpolating $\log L_i$ between bracketing times $t_i < t < t_{i+1}$ or fixed to L_N/T_N for $t > t_N$. The visual optical depth $\tau_{V,i}$ is determined at grid points $i = 1 \cdots (N-1)$, but fixed to the optical depth of the progenitor wind outside the current dust radius

$$\tau_V(r_d) = \frac{R(\tau_V = 1)}{r_d(t)} \tag{A1}$$

for $t > t_N$, where the dust radius declines exponentially starting from radius r_0 on time scale t_0, and then begins to expand outwards at the shock velocity v_s,

$$r_d(t) = r_0 \exp(-t/t_0) + v_s t. \tag{A2}$$

Thus, the last optical depth grid point is $\tau_{V,N} = \tau_V(r_d(t_N))$ and represents the point where the optical depth of the wind outside the shock has fully reformed. The parameters of the model are then the N luminosities

L_i and temperatures T_i, the $N-1$ optical depth points $\tau_{V,i}$ ($i = 1 \cdots N-1$) and times t_i ($i = 2 \cdots N$), the shock velocity v_s, the dust radius parameters r_0 and t_0, the $\tau_V = 1$ radius of the progenitor wind $R(\tau_V = 1)$, and Q_{rat}, which enters into the estimated dust temperature and is a proxy for the more complicated radiation transfer of the DUSTY models.

The emission has four components: a shock break out of luminosity L_{peak}, duration r_*/c, and temperature $T_{peak} = 50000$ K; an optical transient of luminosity $L_O = L(t) - L_N$; a shock with luminosity $L_S = L_N$; and, finally, the luminosity absorbed and re-radiated by the dust L_D. We model the optical contributions as a black bodies, where it is useful to define

$$\hat{B}_\nu(n,T) = \lambda^{-n} B_\nu(T) \left[\int d\nu \lambda^{-n} B_\nu(T) \right]^{-1}, \tag{A3}$$

a modified Planck function normalized to unit total luminosity, and let $f(\lambda) = \tau_\lambda/\tau_V$ be the optical depth ratio in the DUSTY models between the visual optical depth τ_V and that at wavelength λ, τ_λ. The escaping radiation from the transient is then

$$L_{\nu,O}(t) = L_0 \hat{B}_\nu(0, T(t)) e^{-\tau_V(t) f(\lambda)} \tag{A4}$$

and the fraction of the optical transient luminosity escaping is

$$f_{O,esc} = \int d\nu B_\nu(0, T(t)) e^{-\tau_V(t) f(\lambda)} \tag{A5}$$

The shock luminosity is assumed to be initially generated as X-rays at the energy of Eqn. 17, and then absorbed by the wind exterior to the shock using the density profile set by the progenitor optical depth, $\rho = R(\tau_V = 1)/\kappa r^2$, and the X-ray opacities of Eqn. 21. The escape fractions were computed for fixed wind densities and velocities of $v_s = 1100$ and 560 km/s, respectively. Let $f_{X,abs}$ be the fraction of the X-rays energy which is absorbed. We also apply the correction from Eqn. 13 for the balance between cooling and expansion losses. Thus, the shock energy absorbed in the wind is

$$L_{X,abs} = L_S f_{X,abs} \left[1 + t_{exp}/t_{cool} \right]^{-1}. \tag{A6}$$

In the simple model, we just treat this in the same manner is the radiation from the optical transient, where it contributes

$$L_{\nu,X}(t) = L_{X,abs} \hat{B}_\nu(0, T(t)) e^{-\tau_V(t) \tau_R(\lambda)} \tag{A7}$$

by direct emission and with the same fraction absorbed by dust. The shock model discussed in §4.4 uses a list of emission lines and the fraction of energy radiated in each line from Allen et al. (2008) as the model for the spectrum produced by the absorbed X-rays, and computes the extinction and fraction absorbed based on the model line spectrum. Finally, the shock breakout luminosity was set by

$$L_{peak} = 16\pi r_0^2 Q_{rat} \sigma T_{dest}^4 \tag{A8}$$

with $T_{dest} = 1500$ K, heating the dust at radius r_0 to T_{dest}. We used a fixed temperature of $T_{peak} = 50000$ K and gave it a duration comparable to the light crossing time of the progenitor r_*/c with $r_* = 5 \times 10^{13}$ cm. We only consider the "dust echo" from the breakout peak and ignore the short UV flash.

The dust luminosity is then

$$L_d(t) = (L_{peak}(t) + L_0(t) + L_{X,abs}(t))(1 - f_{O,esc}) \quad \text{(A9)}$$

and the dust temperature is

$$T_d = \left(\frac{L_{peak}(t) + L_0(t) + L_{X,abs}(t)}{16\pi\sigma Q_{rat} r_d(t)^2} \right)^{1/4}, \quad \text{(A10)}$$

including the factor Q_{rat} (average ratios of Planck factors) to make it easier to match this model to the DUSTY results. We then used a modified Planck function for the SED of the dust emission,

$$L_{\nu,d} = L_d \hat{B}_\nu(1, T_d). \quad \text{(A11)}$$

We then include the effects of light travel time ("dust echoes") on the dust emissions, spreading the contribution of the emission from any time t uniformly over the interval $t < t' < t + 2r(t)/c$, so the total emission is

$$L_\nu = L_{\nu,O}(t) + L_{\nu,X}(t) + \langle L_{\nu,d}(t') \rangle. \quad \text{(A12)}$$

We also experimented with including direct emission from the progenitor, modeled as a black body with the luminosities from §2 and a temperature of 3000 K. The models were then fit to the light curve data, with priors to match the parameters of the DUSTY models for $R(\tau_V = 1)$ in the progenitor models and the sequence of luminosity, optical depth and dust radius estimates in the transient models. The shock velocity was constrained to match the estimates by Smith et al. (2010) to 10% and the "Planck" term was constrained to have $\log Q_{rat} = 0$ to 10%.

REFERENCES

Abia, C., & Isern, J. 2000, ApJ, 536, 438

Allen, M. G., Groves, B. A., Dopita, M. A., Sutherland, R. S., & Kewley, L. J. 2008, ApJS, 178, 20

Andrews, J. E., et al. 2010, ApJ, 715, 541

Andrews, J. E., et al. 2011, ApJ, 731, 47

Arbour, R., & Boles, T. 2008, Central Bureau Electronic Telegrams, 1234, A260000

Berger, E., & Chornock, R. 2010, The Astronomer's Telegram, 2638, 1

Berger, E., & Soderberg, A. 2008, The Astronomer's Telegram, 1544, 1

Berger, E., et al. 2009, ApJ, 699, 1850

Bond, H. E., Walter, F. M., & Velasquez, J. 2008, IAU Circ., 8946, 2

Bond, H. E., Bedin, L. R., Bonanos, A. Z., Humphreys, R. M., Monard, L. A. G. B., Prieto, J. L., & Walter, F. M. 2009, ApJ, 695, L154

Botticella, M. T., et al. 2009, MNRAS, 398, 1041

Canizares, C. R., Kriss, G. A., & Feigelson, E. D. 1982, ApJ, 253, L17

Chandra, P., & Soderberg, A. 2008, The Astronomer's Telegram, 1382, 1

Chevalier, R. A. 1982, ApJ, 258, 790

Chevalier, R. A., & Fransson, C. 1994, ApJ, 420, 268

Chevalier, R. A., Fransson, C., & Nymark, T. K. 2006, ApJ, 641, 1029

Chugai, N. N. 1992, Soviet Ast., 36, 63

Chugai, N. N., & Danziger, I. J. 1994, MNRAS, 268, 173

Draine, B. T. 1981, ApJ, 245, 880

Draine, B. T., & Lee, H. M. 1984, ApJ, 285, 89

Draine, B. T., & Woods, D. T. 1991, ApJ, 383, 621

Dwek, E. 1983, ApJ, 274, 175

Dwek, E. 1985, ApJ, 297, 719

Falk, S. W., & Arnett, W. D. 1977, A&AS, 33, 515

Fesen, R. A., & Matonick, D. M. 1994, ApJ, 428, 157

Fransson, C. 1982, A&A, 111, 140

Gieren, W., Pietrzyński, G., Soszyński, I., Bresolin, F., Kudritzki, R.-P., Minniti, D., & Storm, J. 2005, ApJ, 628, 695

Gogarten, S. M., Dalcanton, J. J., Murphy, J. W., Williams, B. F., Gilbert, K., & Dolphin, A. 2009, ApJ, 703, 300

Groenewegen, M. A. T., Sloan, G. C., Soszyński, I., & Petersen, E. A. 2009, A&A, 506, 1277

Hoffman, D., et al. 2011, The Astronomer's Telegram, 3160, 1

Humphreys, R. M., et al. 1997, AJ, 114, 2778

Ivezic, Z., & Elitzur, M. 1997, MNRAS, 287, 799

Ivezic, Z., Nenkova, M., & Elitzur, M. 1999, User Manual for DUSTY, University of Kentucky Internal Report http:www.pa.uky.edu̅oshedusty

Ivezić, Ž., & Elitzur, M. 2010, MNRAS, 404, 1415

Kashi, A., Frankowski, A., & Soker, N. 2010, ApJ, 709, L11

Kasliwal, M. M., et al. 2011, ApJ, 730, 134

Khan, R., Stanek, K. Z., Prieto, J. L., Kochanek, C. S., Thompson, T. A., & Beacom, J. F. 2010, ApJ, 715, 1094

Kulkarni, S. R., et al. 2007, Nature, 447, 458

Lundqvist, P., & Fransson, C. 1988, A&A, 192, 221

Mathis, J. S., Rumpl, W., & Nordsieck, K. H. 1977, ApJ, 217, 425

Matsuura, M., et al. 2009, MNRAS, 396, 918

Monard, L. A. G. 2008, IAU Circ., 8946, 1

Ofek, E. O., et al. 2010, ApJ, 724, 1396

Ohsawa, R., et al. 2010, ApJ, 718, 1456

Pastorello, A., et al. 2004, MNRAS, 347, 74

Patat, F., Maund, J. R., Benetti, S., Botticella, M. T., Cappellaro, E., Harutyunyan, A., & Turatto, M. 2010, A&A, 510, A108

Poelarends, A. J. T., Herwig, F., Langer, N., & Heger, A. 2008, ApJ, 675, 614

Prieto, J. L. 2008, The Astronomer's Telegram, 1550, 1

Prieto, J. L., et al. 2008b, ApJ, 681, L9

Prieto, J. L., Sellgren, K., Thompson, T. A., & Kochanek, C. S. 2009, ApJ, 705, 1425

Prieto, J. L., et al. 2010, The Astronomer's Telegram, 2406, 1

Prieto, J. L., Szczygiel, D. M., Kochanek, C. S., Stanek, K. Z., Thompson, T. A., Beacom, J. F., Garnavich, P. M., & Woodward, C. E. 2010, arXiv:1007.0011

Pumo, M. L., et al. 2009, ApJ, 705, L138

Rybicki, G. B., & Lightman, A. P. 1979, New York, Wiley-Interscience, 1979

Sahu, D. K., Anupama, G. C., Srividya, S., & Muneer, S. 2006, MNRAS, 372, 1315

Schlegel, D. J., Finkbeiner, D. P., & Davis, M. 1998, ApJ, 500, 525

Schlegel, E. M., Ryder, S., Staveley-Smith, L., Petre, R., Colbert, E., Dopita, M., & Campbell-Wilson, D. 1999, AJ, 118, 2689

Schure, K. M., Kosenko, D., Kaastra, J. S., Keppens, R., & Vink, J. 2009, A&A, 508, 751

Smith, N., et al. 2009, ApJ, 697, L49

Smith, N., Li, W., Silverman, J. M., Ganeshalingam, M., & Filippenko, A. V. 2010, arXiv:1010.3718

Steele, T. N., Silverman, J. M., Ganeshalingam, M., Lee, N., Li, W., & Filippenko, A. V. 2008, Central Bureau Electronic Telegrams, 1275, A260000

Thompson, T. A., Prieto, J. L., Stanek, K. Z., Kistler, M. D., Beacom, J. F., & Kochanek, C. S. 2009, ApJ, 705, 1364

Umana, G., Buemi, C. S., Trigilio, C., Leto, P., & Hora, J. L. 2010, ApJ, 718, 1036

Waxman, E., Mészáros, P., & Campana, S. 2007, ApJ, 667, 351

Wesson, R., et al. 2010, MNRAS, 403, 474

Wright, E. L. 1980, ApJ, 242, L23

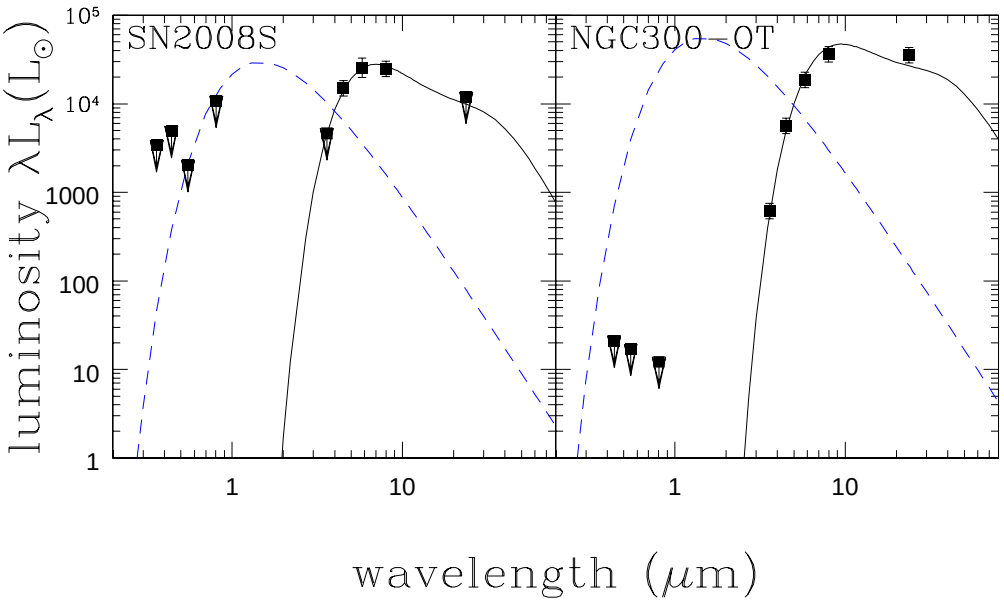

Fig. 1.— The spectral energy distributions of the SN 2008S (left) and NGC 300-OT (right) progenitors modeled as DUSTY winds. The underlying star is assumed to be a cold, T_* = 2500 K, extreme AGB star, (badly) modeled with the black body SED shown by the dashed lines. Note, however, that no particular stellar temperature is required by the models because of the high optical depths. The solid curves show the DUSTY wind model for the observed SED assuming an inner edge dust temperature of 1500 K. The models have visual optical depths of τ_V = 300 and 750, respectively, and stellar luminosities of $L_* = 10^{4.6} L_\odot$ and $10^{4.9} L_\odot$. The SN 2008S data are from Prieto et al. (2008b), the NGC 300-OT mid-IR data are from Prieto (2008a) (also Thompson et al. (2009)) and the NGC 300-OT optical limits are from Berger & Soderberg (2008) (also Berger et al. (2009) and Bond et al. (2009)).

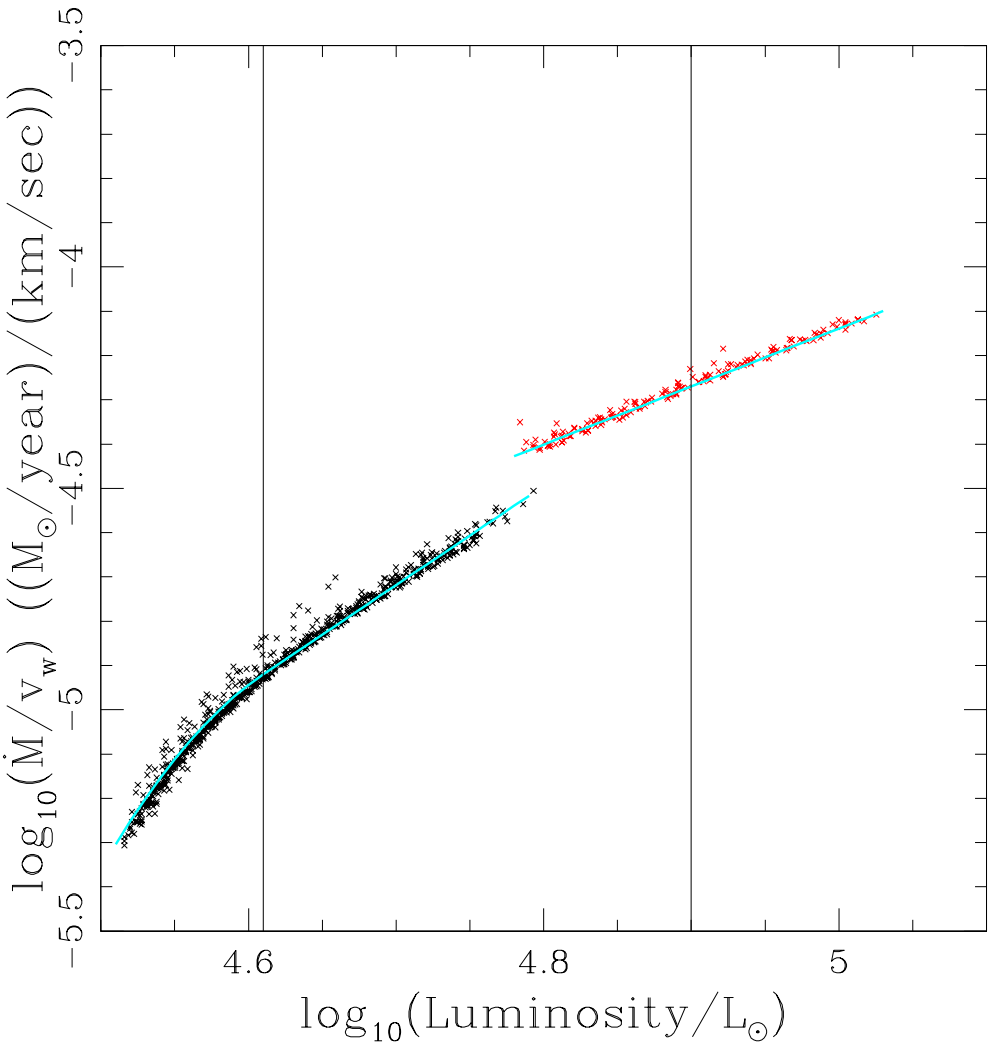

Fig. 2.— The stellar luminosity and wind density parameters for DUSTY models of the progenitors of SN 2008S (left, black) and the NGC 300-OT (right, red). These include all models roughly consistent with the photometry and having inner edge dust temperatures $\geq$ 1000 K. The cyan curve shows the wind density predicted from the radius $R(\tau_V = 1)$ where the visual optical depth is unity and a dust optical depth of $\tau_V = 137$ cm^2/g. This is for DUSTY's default gas-to-dust ratio of $r_{gd} = 200$, and the wind density can be raised as $\dot{M}/v_w \propto r_{gd}$ by reducing the dust opacity per unit mass, $\kappa_V \propto r_{gd}^{-1}$, or *vice versa*.

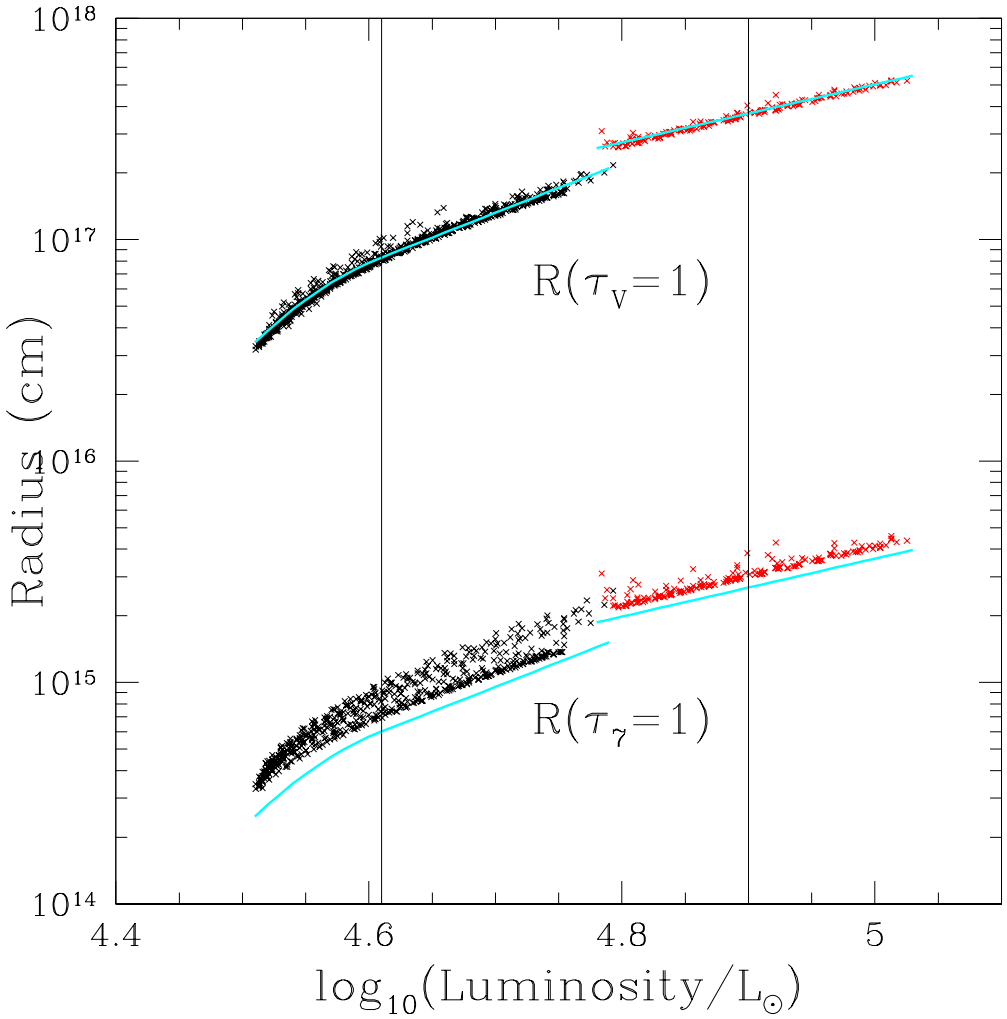

Fig. 3.— The radii $R(\tau_V = 1)$ and $R(\tau_7 = 1)$ where the visual optical (upper points) and 7μm (lower points) optical depth is unity for the SN 2008S (left, black) and the NGC 300-OT (right, red) progenitor winds. The vertical lines show the model likelihood-weighted mean luminosities. The cyan line through the $R(\tau_V = 1)$ points shows the simple fits given in Eqn. 2, while the line just below the $R(\tau_7 = 1)$ points show the prediction for that radius given a simple $\rho \propto 1/r^2$ wind model.

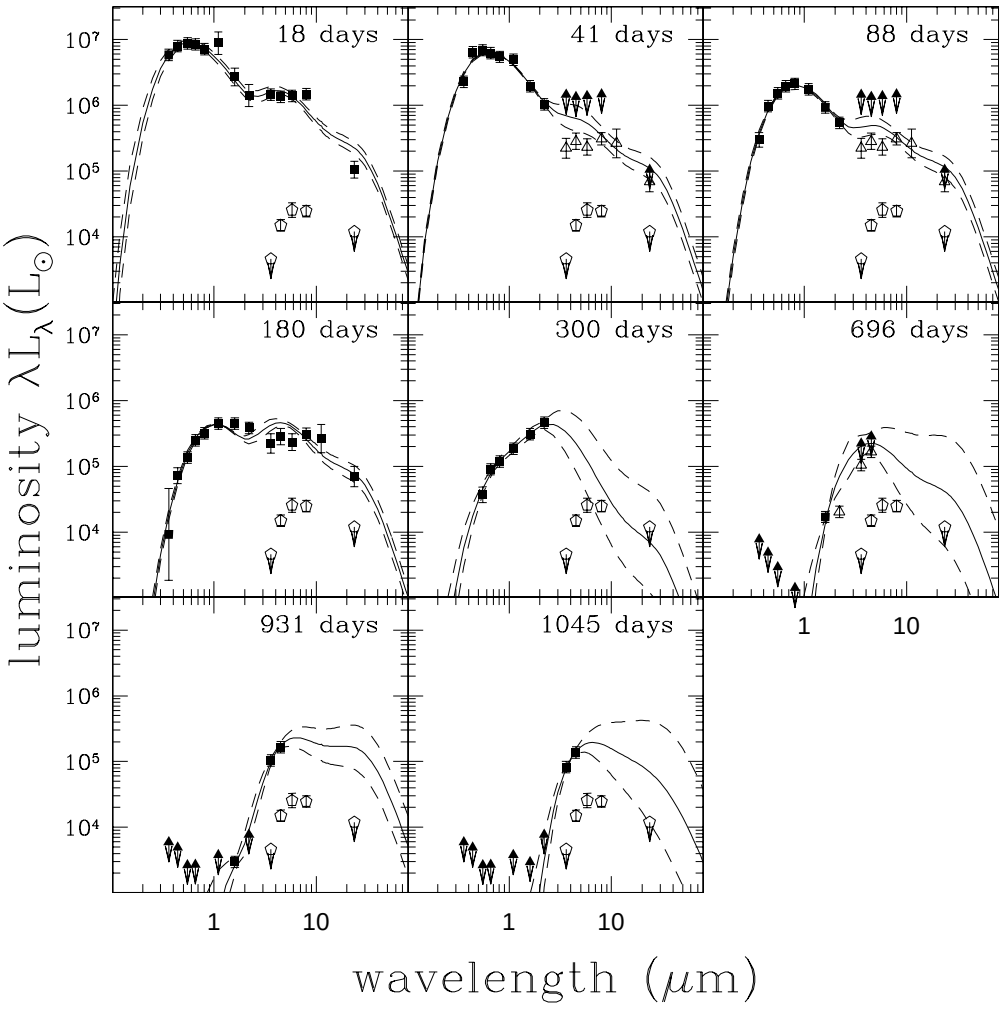

Fig. 4.— The evolving SEDs of SN 2008S. Filled squares show measurements at that epoch. Filled triangles show upper bounds either from that epoch or a plausible bound set by the other epochs. Open triangles show plausible lower bounds set by the other epochs. The open pentagons show the SED of the progenitor star excluding the optical upper limits for clarity. The solid line shows the probability-weighted mean SED of the DUSTY models and the dashed line shows the dispersion of these SEDs. Epochs are relative to the same reference date as used by Botticella et al. (2009).

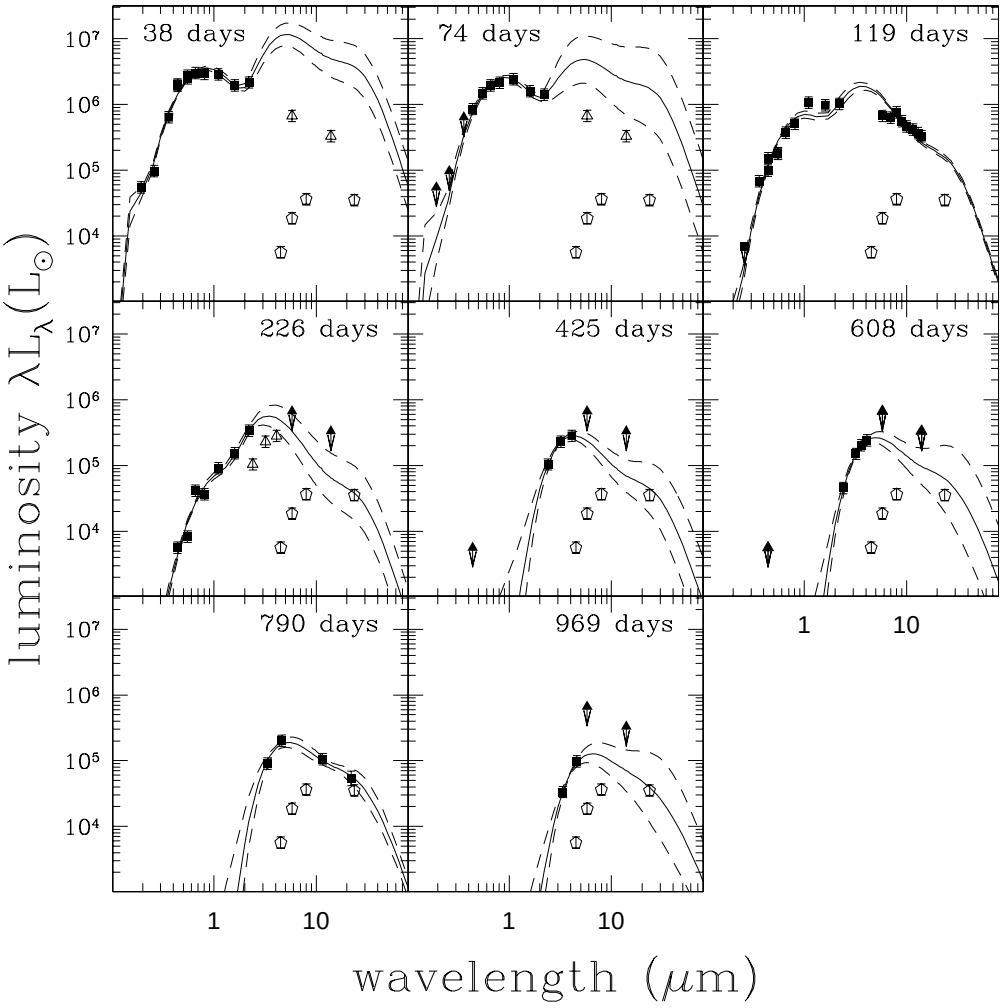

Fig. 5.— The evolving SEDs of the NGC 300-OT. Filled squares show measurements at that epoch. Filled triangles show upper bounds either from that epoch or a plausible bound set by the other epochs. Open triangles show plausible lower bounds set by the other epochs. The open pentagons show the SED of the progenitor star excluding the optical upper limits for clarity. The solid line shows the probability-weighted mean SED of the DUSTY models and the dashed line shows the dispersion of these SEDs. The optical limit from Prieto et al. (2010) is applied to the last two epochs but lies below the lower edge. Epochs are relative to 17 April 2008.

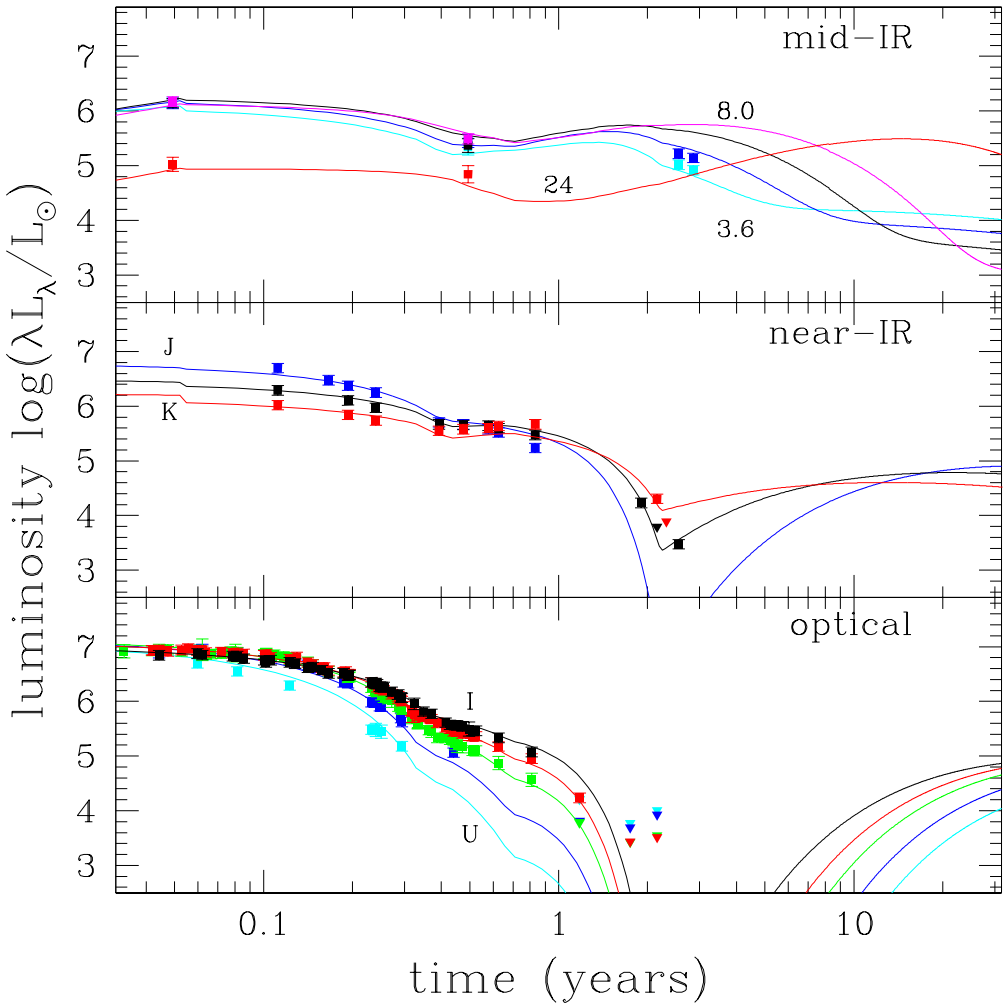

Fig. 6.— Simple light curve models for SN 2008S. The top, middle and bottom panels show the mid-IR (IRAC 3.6, 4.5, 5.8, 8.0 and MIPS 24μm), near-IR (J, H and K), and optical (UBVRI) light curves along with the simple model fits. Measurements are shown by filled squares, upper bounds by triangles. The late time optical/near-IR light curves primarily illustrate the time scales on which the absorption exterior to the shock becomes negligible – while correct for overall energetics, they are wrong in detail because they (incorrectly) assume that the SED of the shock emission is the same as the black body SED of the optical transient.

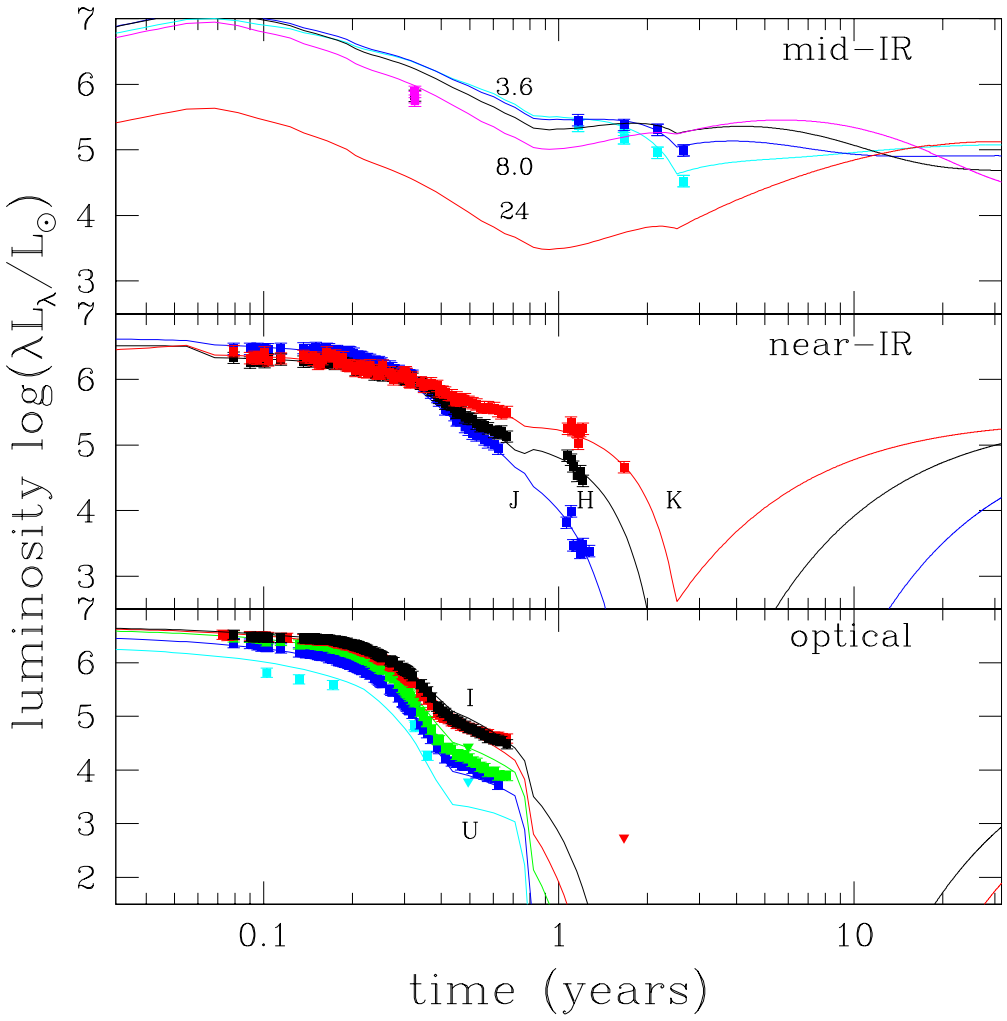

Fig. 7.— Simple light curve models for the NGC 300-OT. The top, middle and bottom panels show the mid-IR (IRAC 3.6, 4.5, 5.8, 8.0 and MIPS 24μm), near-IR (J, H and K), and optical (UBVRI) light curves along with the simple model fits. Measurements are shown by filled squares, upper bounds by triangles. Models allowing modest changes in the transient temperature better fit the "kink" in the optical light curves. The same caveats apply here as in Fig. 6. The poorer fit for the R band is probably due to Hα emission.

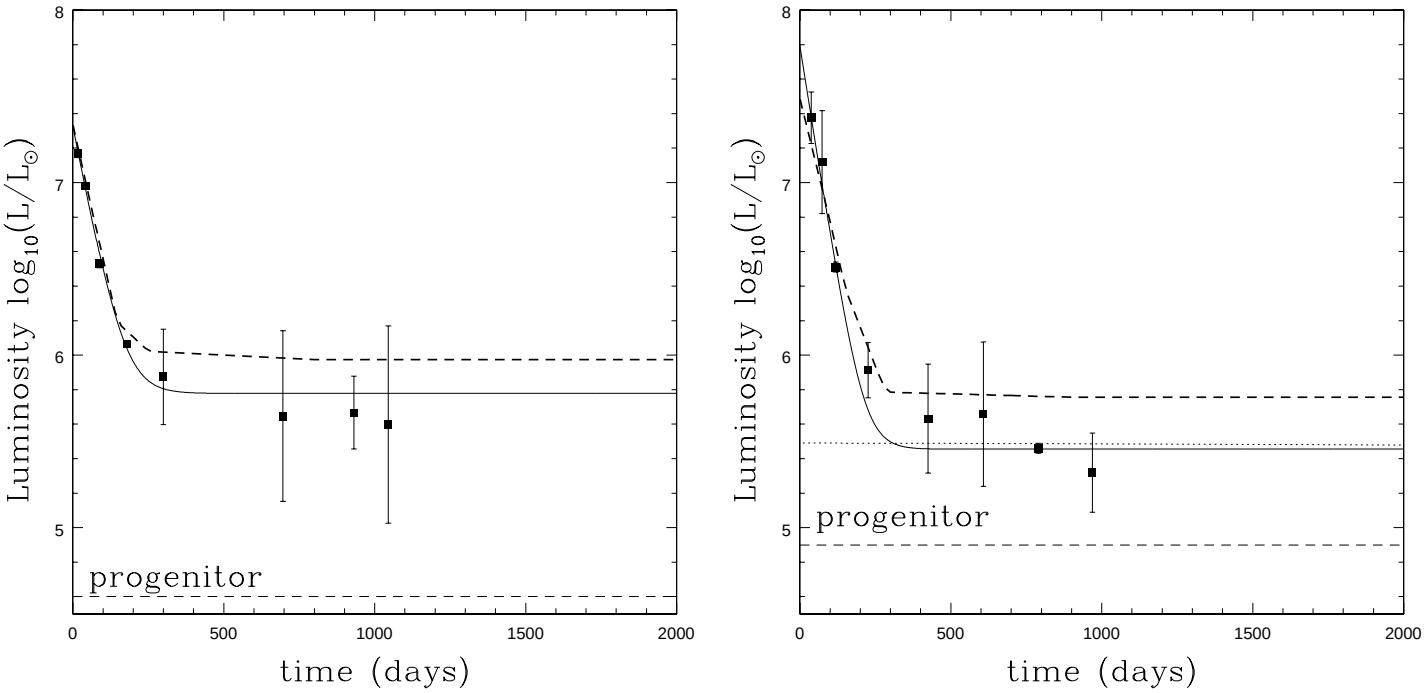

Fig. 8.— The luminosity evolution of SN 2008S (left) and the NGC 300-OT (right). The points show the luminosity estimates from the DUSTY models. The solid curve shows a simple exponential plus constant model for the luminosity, while the heavy dashed curve shows the model from the light curve fits. The dashed curve shows the luminosity of the progenitor.

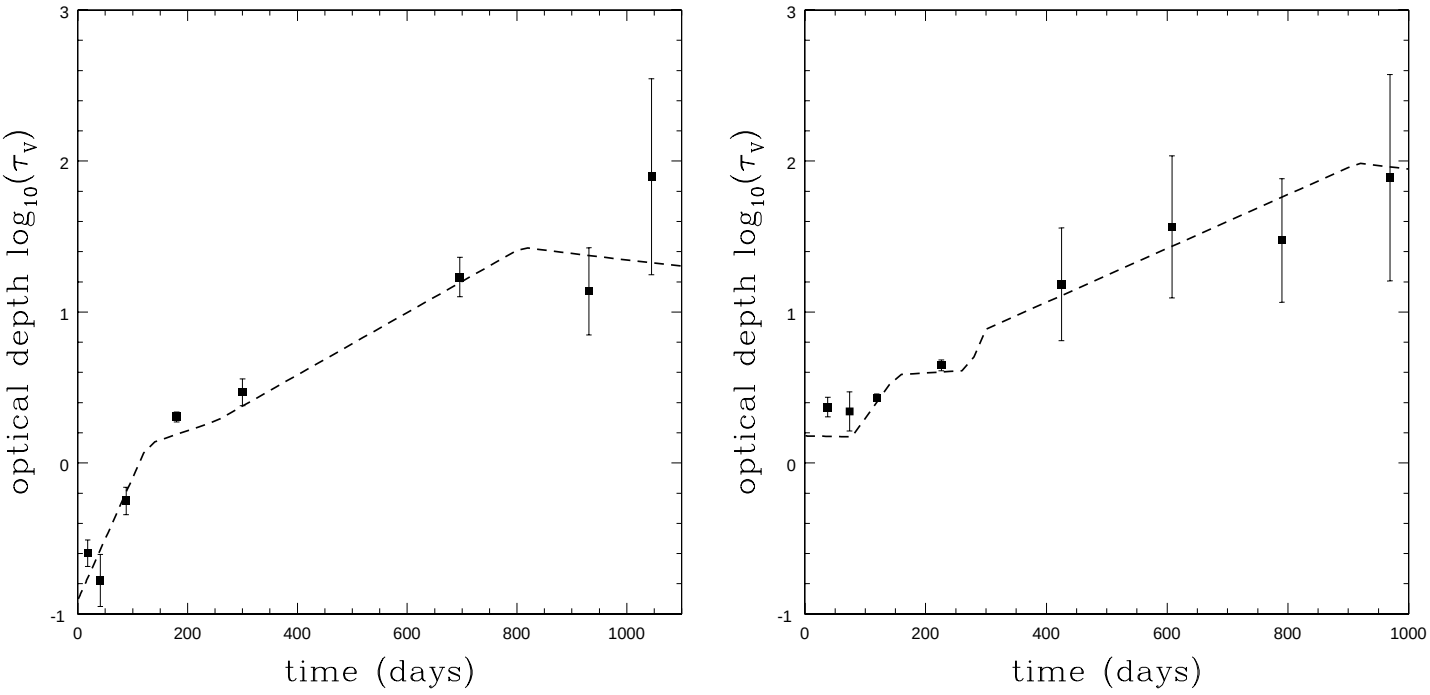

Fig. 9.— The optical depth evolution of SN 2008S (left) and the NGC 300-OT (right). The points show the τ_V estimates from the DUSTY models, while the heavy dashed curve shows the results from the light curve fits.

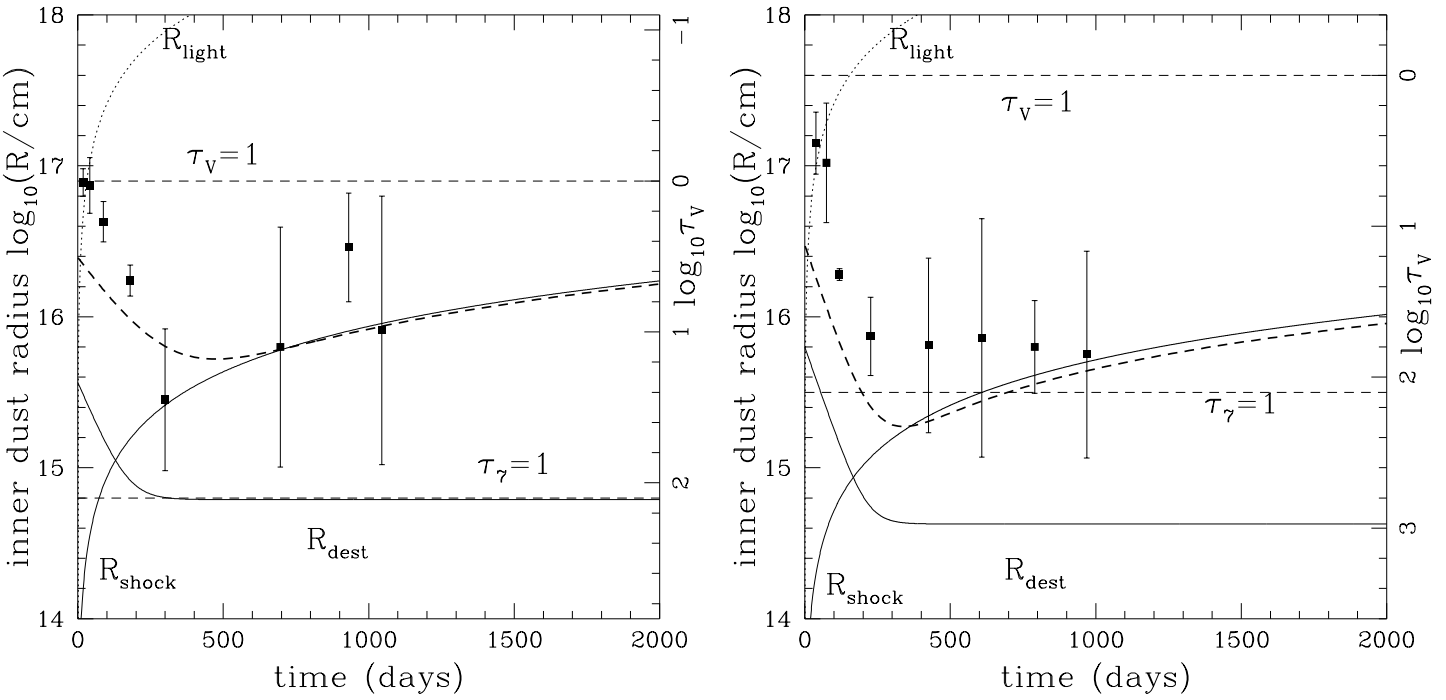

Fig. 10.— The dust radius evolution of SN 2008S (left) and the NGC 300-OT (right). The points show the radius of the inner edge of the dust from the DUSTY models while the heavy dashed line shows the model from the light curve fits. The right axis shows the visual optical depth scale of the progenitor wind, where the horizontal dashed lines mark the radii where the visual (τ_V = 1) and 7μm (τ_7 = 1) optical depths to infinity were unity. The solid lines show the small grain dust destruction radius R_{dest} from Eqn. 14 predicted from the luminosity model in Fig. 8, and the shock radius $R_{shock} = v_s t$ assuming velocities of v_s = 1000 and 600 km/s for SN 2008S and the NGC 300-OT, respectively. The dotted line shows the light radius $R_{light} = ct$. Epochs above this line will be affected by finite light crossing times, although not significantly on the logarithmic scales of Figs. 8, 9 and 10.

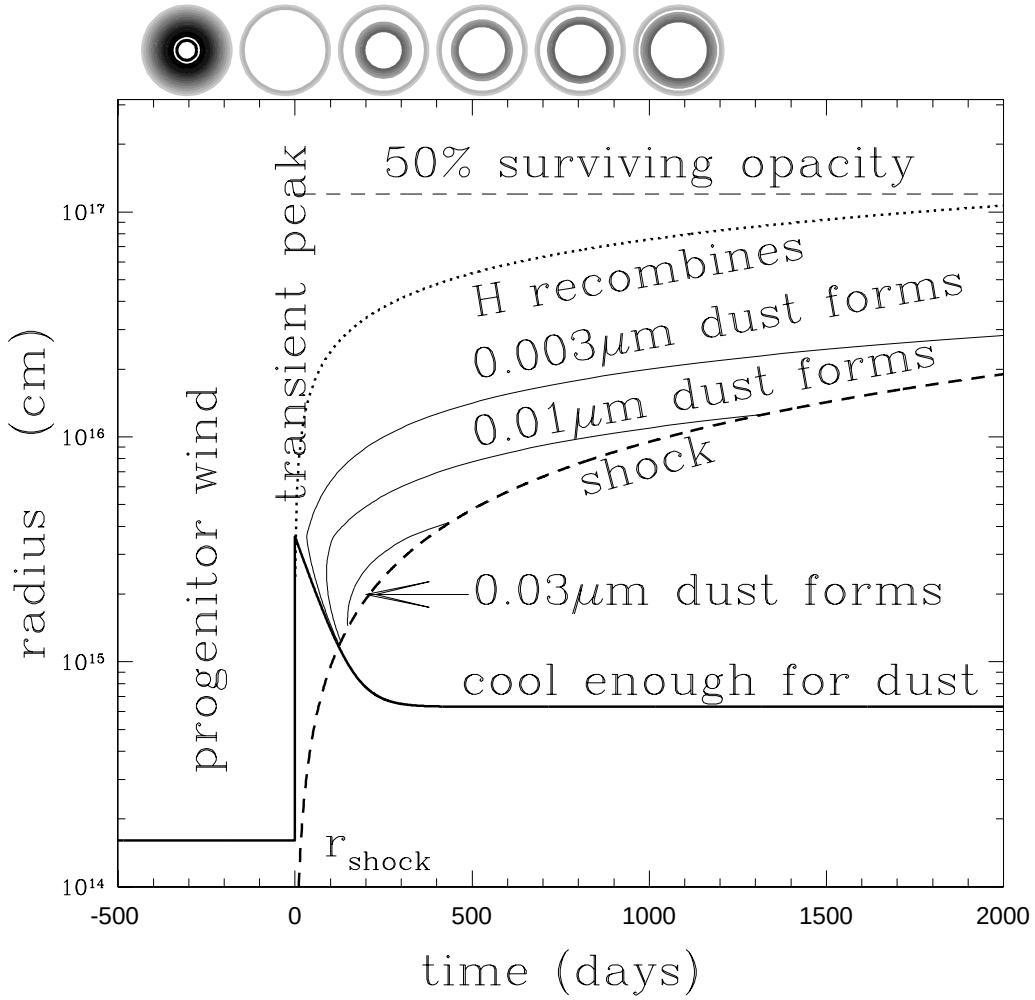

Fig. 11.— Physical scales relevant for dust formation as a function of time and scaled for SN 2008S. The heavy solid line shows the radius R_{form} (Eqn. 14) interior to which small grains would be destroyed. The heavy dashed line shows the radius of the outgoing shock. The horizontal dashed line shows the radius at which 50% of the dust opacity would be destroyed given a shock break out luminosity of $4 \times 10^{10} L_{\odot}$ (Eqn. 5). The dotted shows the radius interior to which hydrogen can have recombined. Finally, the light black lines show the radii interior to which grains can have regrown to 0.003μm, 0.01μm, and 0.03μm, respectively. These would move outwards in radius by a factor of two for the coagulation model. The cartoons at the top roughly illustrate where dust is located and its evolution in radius and optical depth.

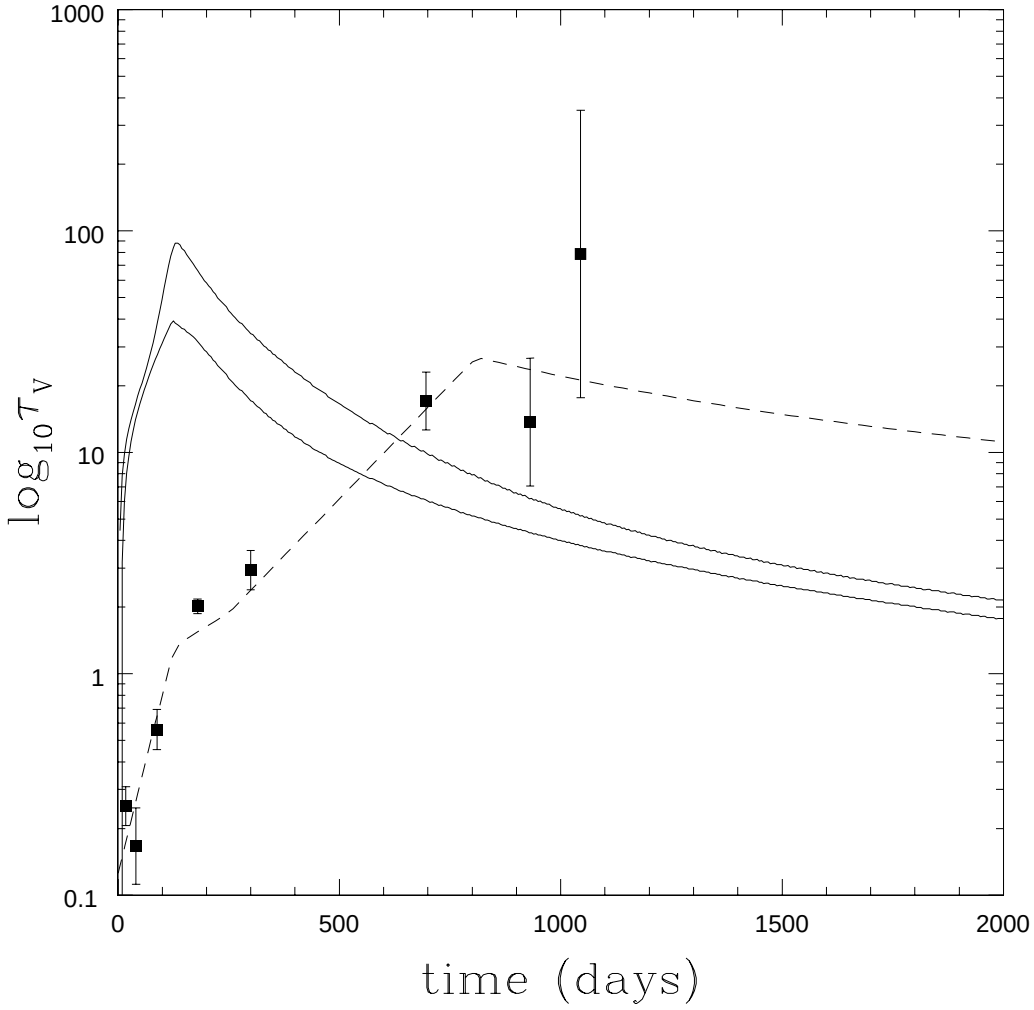

Fig. 12.— Simple models for the reformation of dust in the wind of SN 2008S (solid curves). The lower curve assumes the growth time scale of Eqn. 15, and the upper curve assumes a rate 4 times faster, corresponding to growth by coagulation rather than monomer accretion. The points and dashed curve show the optical depth estimates from the fits to the SEDs and the lightcurves, respectively, as in Fig. 9. Given the simplicity of the models, only qualitative agreement is to be expected.

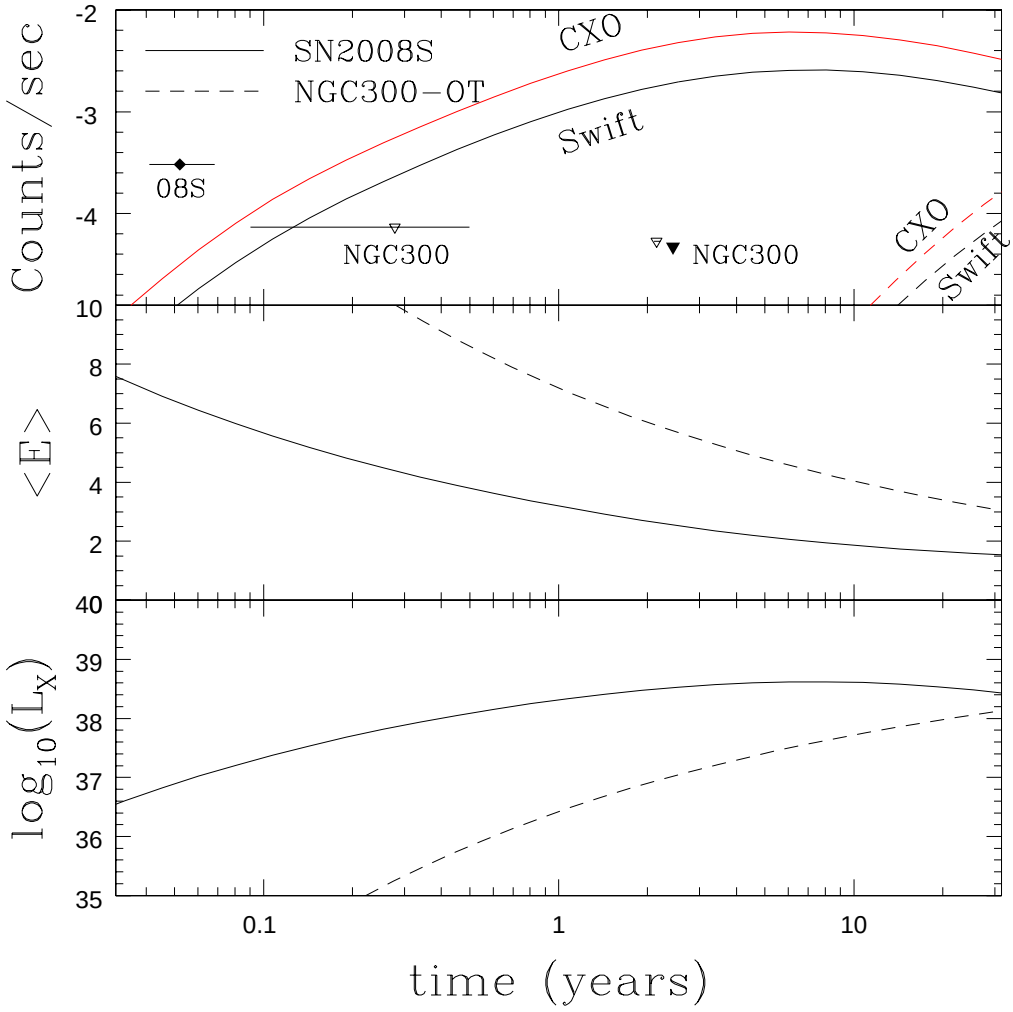

Fig. 13.— The predicted X-ray properties of SN 2008S (solid) and the NGC 300-OT (dashed). The bottom panel shows the estimated luminosity including both absorption and the crude estimate of the balance between radiation and expansion. The middle panel shows the mean X-ray energy after absorption. The top panel shows estimates of the count rates for SWIFT (lower count rates, black) and Chandra (higher count rates, red). The points show the count rates for finding 3 counts in archival SWIFT (black diamond for SN 2008S open triangles for the NGC 300-OT) and Chandra (filled triangle for the NGC 300-OT) observations given their integration times. Multiple SWIFT epochs were combined into a single limit.

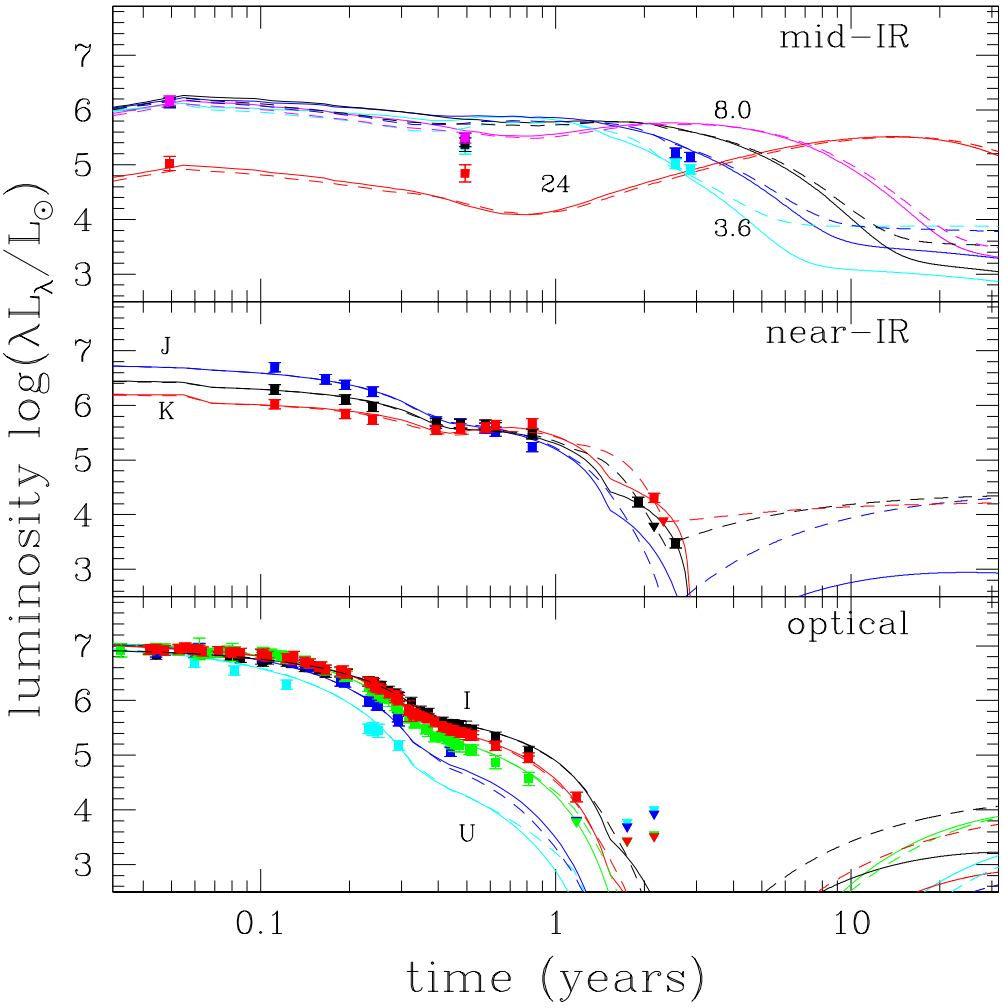

Fig. 14.— Alternate light curve models for SN 2008S. As in Fig. 6, the top, middle and bottom panels show the mid-IR (IRAC 3.6, 4.5, 5.8, 8.0 and MIPS 24μm), near-IR (J, H and K), and optical (UBVRI) light curves. The solid lines show the light curves using an emission line model for the shock spectrum, and the dashed lines add an unobscured 3000 K black-body with the luminosity of the progenitor. As expected, the differences between the models appear in the near-IR and optical as the optical depth to the shock front diminishes. The shock model has relatively little near-IR emission, so the near-IR emission never recovers, while the shock plus progenitor model is brighter in the near-IR than the original model because of the cooler progenitor black body temperature. The latter model assumes that there is no significant dust optical depth interior to the shock.